AD-A133 744 FOCUSED ACOUSTICAL AND OPTICAL BACKSCATTERING FROM SPHERES AND PROPERTIES..(U) WASHINGTON STATE UNIV PULLMAN DEPT OF PHYSICS P L MARSTON 15 SEP 83 TR-3 1/*

UNCLASSIFIED N00014-80-C-0838 F/G 20/6 NL

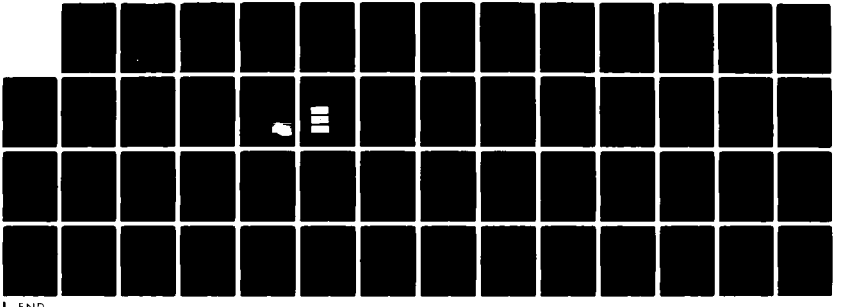

END

DATE FILMED

DTIC

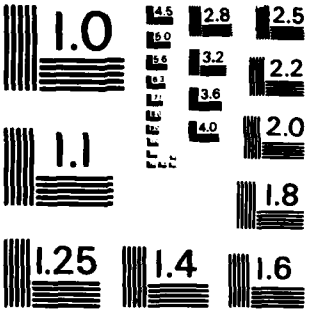

TECHNICAL REPORT NO. 3

FOCUSED ACOUSTICAL AND OPTICAL BACKSCATTERING FROM SPHERES AND PROPERTIES OF OPTOACOUSTIC SOURCES

by

Philip L. Marston

September 15, 1983

DEPARTMENT OF PHYSICS
WASHINGTON STATE UNIVERSITY

12

DEPARTMENT OF PHYSICS

WASHINGTON STATE UNIVERSITY

PULLMAN, WA 99164-2814

TECHNICAL REPORT NO. 3

FOCUSED ACOUSTICAL AND OPTICAL BACKSCATTERING FROM SPHERES AND PROPERTIES OF OPTOACOUSTIC SOURCES

by

Philip L. Marston

September 15, 1983

Prepared for:

OFFICE OF NAVAL RESEARCH

CONTRACT NO. N00014-80-C-0838

Unclassified

SECURITY CLASSIFICATION OF THIS PAGE (When Data Entered)

REPORT DOCUMENTATION PAGE		READ INSTRUCTIONS BEFORE COMPLETING FORM
1. REPORT NUMBER N00014-80-C-0838-TR3	2. GOVT ACCESSION NO. AD-A133 744	3. RECIPIENT'S CATALOG NUMBER
4. TITLE (and Subtitle) FOCUSED ACOUSTICAL AND OPTICAL BACKSCATTERING FROM SPHERES AND PROPERTIES OF OPTOACOUSTIC SOURCES		5. TYPE OF REPORT & PERIOD COVERED Interim Technical Report 1 Sept 82 - 31 Aug 83 6. PERFORMING ORG. REPORT NUMBER
7. AUTHOR(s) Philip L. Marston		8. CONTRACT OR GRANT NUMBER(s) N00014-80-C-0838
9. PERFORMING ORGANIZATION NAME AND ADDRESS Department of Physics Washington State University Pullman, WA 99164-2814		10. PROGRAM ELEMENT, PROJECT, TASK AREA & WORK UNIT NUMBERS
11. CONTROLLING OFFICE NAME AND ADDRESS Physics Division Office Office of Naval Research Arlington, VA 22217		12. REPORT DATE 15 September 1983 13. NUMBER OF PAGES 52
14. MONITORING AGENCY NAME & ADDRESS(if different from Controlling Office)		15. SECURITY CLASS. (of this report) Unclassified 15a. DECLASSIFICATION/DOWNGRADING SCHEDULE

16. DISTRIBUTION STATEMENT (of this Report)

Approved for public release; distribution unlimited.

17. DISTRIBUTION STATEMENT (of the abstract entered in Block 20, if different from Report)

18. SUPPLEMENTARY NOTES

Contains reprints and preprints listed in block 20.

19. KEY WORDS (Continue on reverse side if necessary and identify by block number)

Acoustic scattering, Inverse scattering, Elastic-wave scattering, Backscattering, Sonar calibration, Physical acoustics, Underwater acoustics, Light scattering, Bubbles, Mie theory, Optical oceanography, Fog, Light extinction, Optoacoustics, Photoacoustics, Half-order derivative

20. ABSTRACT (Continue on reverse side if necessary and identify by block number)

This report consists of publications and preprints on topics related to acoustical and optical scattering and to laser optoacoustic sources of sound. The motivation and interrelation between the topics covered are described in the preface. The authors and titles of the papers enclosed are as follows:

1. P. L. Marston, K. L. Williams, and T. J. B. Hanson, "Observation of the acoustic glory: High-frequency backscattering from an elastic sphere," Journal of the Acoustical Society of America 74, 605-618 (1983).

DD FORM 1 JAN 73 1473 EDITION OF 1 NOV 65 IS OBSOLETE
S/N 0102-LF-014-6601

Unclassified
SECURITY CLASSIFICATION OF THIS PAGE (When Data Entered)

2. P. L. Marston, "Half-order derivative of a sine-wave burst: Applications to two-dimensional radiation, photoacoustics, and focused scattering from spheres and a torus," Journal of the Acoustical Society of America (submitted for publication).

3. P. L. Marston, "Uniform Mie-theoretic analysis of polarized and cross-polarized optical glories," Journal of the Optical Society of America (accepted for publication).

The emphasis of Papers 1 and 2 is on the understanding of the enhanced backscattering from spheres associated with axial focusing. The emphasis on Paper 3 is on the modeling of certain cross-polarization and copolarization effects due to the scattering of laser light from small bubbles in water or from fog.

TABLE OF CONTENTS

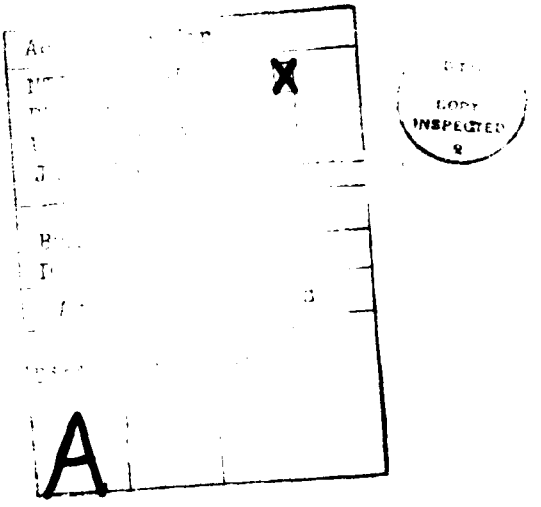

PREFACE

This technical report consists of publications and preprints which are representative of research supported by this contract from September 1982 thru August 1983. The purpose of this preface is to comment on the motivation of, and background for, this research and to interrelate the topics covered.

Paper No. 1 describes the first detailed observations of, and theory for, focused acoustical backscattering from an elastic sphere. This focusing is referred to as "axial focusing" because the scattered pressure is locally enhanced near the backward axis as evidenced by Fig. 9-12. This phenomenon is called the "glory" since the enhanced optical backscattering from cloud droplets (also known as the glory) is caused in part by axial focusing. The first detailed model of transmitted wave glory amplitudes from spheres (acoustical or optical) was developed under this contract.[1] Paper No. 1 contains several theoretical extensions of our previous (fluid sphere) model[1] and it gives data which confirm those extensions. Axially-focused backscattering is potentially significant to sonar technology. Due to the intrinsic isotropy of spheres, there has long been an interest in the use of fluid-filled spherical shells as sonar calibration targets. These targets may also be useful as passive navigational beacons for which backscattering is large for a broad range of frequencies. The theoretical considerations described should facilitate, for the first time, a detailed understanding of focused echoes from large spheres having ka >> 1.

Paper No. 2 describes a detailed calculation of the temporal signatures of axially-focused backscattering from spheres. It is shown that the time-domain response due to axial focusing is describable (under conditions noted) by the "half-order derivative" operator. The effect of this

operator on a sine-wave tone burst is calculated and discussed. The quasi-steady-state approximation used in Paper No. 1 is shown to be applicable for the conditions of that experiment. In addition, axially-focused backscattering from a large torus is modeled. The frequency domain response associated with axial focusing appears to be one of the canonical response functions of acoustics so the temporal response is applicable to several other problems in acoustics, some of which are noted below.

Paper No. 2 also reviews Lighthill's formulation of the pressure radiated from a line source in terms of the half-order derivative operator. A specific example, the transient radiation from certain optoacoustic sources, is considered. When the optical intensity modulation is that of a half-cycle of a sine wave, the calculation displayed in Fig. 5 should approximate the radiated pressure. This calculation (and similar ones for other inputs) should be useful for calibrating broad-band hydrophone systems needed in a study (supported by this contract) of other optoacoustics sources.

Paper No. 3 describes the first uniform analysis (i.e. an analysis which is equally valid for all scattering angles) of a novel measurement configuration for light scattering. The measurement configuration considered is potentially useful for the discrimination of light scattered from spheres (small air bubbles in water or fog droplets) from that of non-spherical particulates. It was previously introduced by us to facilitate the detection of optical glories (i.e. axialy-focused backscattering) from air bubbles in liquids.[2,3] Our previous computations[4,5] and unpublished visual observations indicate that optical glories enhance the near-backward scattering from small air bubbles freely rising in water. (Small bubbles significantly affect the acoustical properties of water and also the air-sea interaction at the ocean's surface.) The calculation described is applicable to the production of cross-

polarized light due to scattering from small bubbles (and from fog or cloud droplets) provided the number density of scatterers is sufficiently small that multiple scattering may be neglected. The calculation is also applicable to non-cross-polarized (sometimes known as copolarized) scattering and to forward as well as backward optical glories.

In other work supported by this contract we have observed the scattering of both white light[6,7] and laser light from bubbles in the vicinity of the critical scattering angle. Color photographs of the white-light scattering are to be published.[7]

In preparing the papers enclosed in this report the principal investigator (P. L. Marston) has benefited from the collaboration with, and/or critical comments by, several students. These include: T. J. B. Hanson, D. S. Langley, B. T. Unger, and K. L. Williams.

P. L. Marston

September 1983

References to Preface

1. P. L. Marston and D. S. Langley, "Glory- and rainbow-enhanced acoustic backscattering from fluid spheres: Models for diffracted axial focusing," Journal of the Acoustical Society of America 73, 1464-1475 (1983).

2. D. S. Langley and P. L. Marston, "Glory in the Optical Backscattering from Air Bubbles," Physical Review Letters 47, 913-916 (1981).

3. P. L. Marston and D. S. Langley, "Glory in backscattering: Mie and model predictions for bubbles and conditions on refractive index in drops," Journal of the Optical Society of America 72, 456-459 (1982).

4. P. L. Marston, D. S. Langley, and D. L. Kingsbury, "Light scattering by bubbles in liquids: Mie theory, physical-optics approximations, and experiments," Applied Scientific Research 38, 373-384 (1982).

5. P. L. Marston, "Light scattering by bubbles in liquids: comments and applications of results to circularly polarized incident light," Applied Scientific Research 40, 3-5 (1983).

6. P. L. Marston, J. L. Johnson, S. P. Love, and B. L. Brim, "Scattering of white light from a cylindrical bubble: Observations of colors near the critical scattering angle," Technical Digest of the Optical Meeting on Meteorological Optics (Optical Society of America, Washington, D.C., 1983) pp. ThA3-1 - ThA3-4.

7. P. L. Marston, J. L. Johnson, S. P. Love, and B. L. Brim, "Critical angle scattering of white light from a cylindrical bubble in glass: Photographs of colors and computations," Journal of the Optical Society of America (accepted for publication).

Paper Number 1:

Observation of the acoustic glory: High-frequency backscattering from an elastic sphere

Philip L. Marston, Kevin L. Williams, and Timothy J. B. Hanson[a)]

Department of Physics
Washington State University
Pullman, Washington 99164

Reprinted from: J. Acoust. Soc. Am. 74, 605-618 (1983).

Measurements of the scattering of 2.10 MHz ultrasonic bursts gave direct evidence of the acoustic glory. Echo amplitudes were measured as a function of the transverse displacement x from the backward axis; they were maximized on the axis and they manifested side lobes. Except near minima, the amplitudes were proportional to $J_0(kbx/z_n)$ where b and z_n are the radius of, and axial distance to, the virtual focal circles from which the echoes appeared to emanate. This dependence on x is direct evidence of axial focusing (The principal feature of optical glories of drops and bubbles is also axial focusing.). The experiment was performed in water with a fused silica sphere having a radius $a \simeq 51.6$ mm for which $2\pi a/\lambda = ka \simeq 457$. A theory is developed for certain of the echo amplitudes and focal parameters. The theory typically overestimates the amplitudes of the stronger of the echoes by 5%. Appendices describe aspects of the theory not amenable to the experiment, including: (i) a shift of focal parameters which should be significant when $ka \lesssim 100$, and (ii) a distortion of transients described in part by the half-order derivative operator.

a) Present address: Defense Systems Division,
Honeywell, Inc., Hopkins, MN 55343

PACS Nos: 43.20.Fn, 43.20.Px, 43.20.Dk, 42.10.Hc

Observation of the acoustic glory: High-frequency backscattering from an elastic sphere

Philip L. Marston, Kevin L. Williams, and Timothy J. B. Hanson[a)]
Department of Physics, Washington State University, Pullman, Washington 99164

(Received 28 December 1982; accepted for publication 9 May 1983)

Measurements of the scattering of 2.10-MHz ultrasonic bursts gave direct evidence of the acoustic glory. Echo amplitudes were measured as a function of the transverse displacement x from the backward axis; they were maximized on the axis and they manifested side lobes. Except near minima, the amplitudes were proportional to $J_0(kbx/z_n)$, where b and z_n are the radius of, and axial distance to, the virtual focal circles from which the echoes appeared to emanate. This dependence on x is direct evidence of axial focusing. (The principal feature of optical glories of drops and bubbles is also axial focusing.) The experiment was performed in water with a fused silica sphere having a radius $a \simeq 51.6$ mm for which $2\pi a/\lambda = ka \simeq 457$. A theory is developed for certain of the echo amplitudes and focal parameters. The theory typically overestimates the amplitudes of the stronger of the echoes by 5%. Appendices describe aspects of the theory not amenable to the experiment, including: (i) a shift of focal parameters which should be significant when $ka \lesssim 100$, and (ii) a distortion of transients described in part by the half-order derivative operator.

PACS numbers: 43.20.Fn, 43.40.Ey, 43.20.Px, 42.10.Hc

INTRODUCTION

There have been numerous investigations of acoustic backscattering from solid elastic spheres in water.[1-10] (Much of this work is reviewed in Ref. 8.) When the sphere is very large in comparison to an acoustic wavelength, a simple description of the backscattering should be possible by accounting for reflection and the various longitudinal and shear rays internal to the sphere.[9-12] It is insufficient to use elementary ray-optical methods[10] because of a novel focusing effect.[13] Diffraction must be included[9,13] in models of this "axial focusing." It is the purpose of this paper to describe observations of axial focusing of backscattering and to extend a previous model,[13] developed for fluid spheres, to the case of the backscattering of transient signals from elastic spheres. It is demonstrated that the scattering to angles slightly displaced from the exact backward direction can be greatly influenced by the size of the scatterer.

It is appropriate to refer to the scattering described here as the acoustic "glory" because the term "glory" is generally applicable to backscattering from spheres (or other spherically symmetric potentials) when enhanced by axial focusing.[13-15] Axial focusing enhances the amplitudes due to rays backscattered with nonzero impact parameters (the "glory rays") but it does not affect the amplitudes of the axial reflections.[13] There is no axial focusing of the backscattering from cylinders[9-13] and consequently the exact scattering (normalized to that of the geometric reflection from a fixed-rigid object of the same size) is somewhat greater for large elastic spheres than for cylinders.[6,9]

Figure 1 gives a conceptual description of the experiment. A pistonlike transducer of diameter $d = 12.7$ mm is driven electrically so as to produce a tone burst of short duration. The principal burst (neglecting buildup and decay of the transducer's response) is four cycles of a 2.1-MHz sine wave. This corresponds to a wavelength λ of 0.71 mm. The distance z_p from the transducer to the near point of the sphere is 171 cm which is somewhat greater than $3d^2/4\lambda$; consequently, the sphere is in the farfield of the transducer. The sphere is synthetic fused silica[16] with a radius $a = 51.563$ mm. It subtends a half-angle $\simeq a/z_p$ radians (relative to the transducer) which is less than the angle of the first minimum ($\simeq 1.22\lambda/d$ rad) of the farfield radiation. The scattering in near backward directions was monitored with a hydrophone (at the end of a bent hypodermic needle). The hydrophone could be scanned along a line transverse to the symmetry axis. The on-axis distance z to the sphere was always $\ll ka^2$ where $k = 2\pi/\lambda$. Consequently, the hydrophone was not in the farfield scattering region (in the terminology of Ref. 13). For this experiment $ka \simeq 457$. Typically $z \simeq 74$ cm and displacements of the hydrophone from the axis by an amount x of a few millimeters significantly reduced the glory scattering amplitudes.

Principal modifications of the fluid–sphere model (Ref. 13) needed for the description of the experimental results are

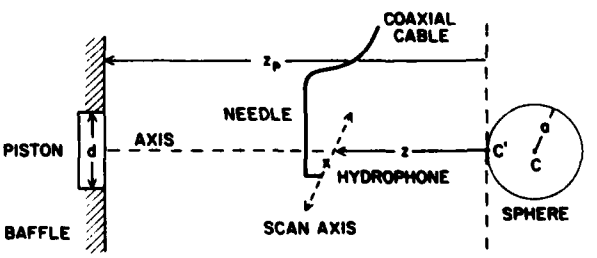

FIG. 1. Simplified diagram of the scattering experiment. The hydrophone may be scanned along a line transverse to the symmetry axis defined by the source and the sphere. The diagram is not drawn to scale.

[a)] Present address: Defense Systems Division, Honeywell, Inc., Hopkins, MN 55343.

 0001-4966/83/080606-14$00.80

description of rays and focal-circle parameters for an elastic sphere; use of reflection and transmission coefficients for water–quartz interface; modeling of nearfield diffractive effects; and discussion of the transient response. The modifications are first developed for the steady-state response. Ray acoustics is used to model amplitudes at planes near the sphere. These amplitudes then propagate (with diffraction) to the hydrophone. Equation numbers from Ref. 13 will be cited with an F prefix. Our nomenclature extends that of Ref. 13.

I. RAYS AND GEOMETRIC FOCAL-CIRCLE PARAMETERS

Backscattered ray paths through large elastic cylinders[11,12] and spheres[10] depend on the following integer parameters: n, the total number of ray traverses of the interior; m, the number of traverses as a shear wave; $n-m$, the number of traverses as a longitudinal wave; and l, where $2l-1$ is the number of times internal chords cross the axis shown in Fig. 1. (The parameter n' of Ref. 13 is $l-1$.) To simplify the description of focal-circle parameters, the following approximations will be made: (i) the incident wave will be taken to be a plane wave, and (ii) the geometric condition on glory rays will be that they leave the sphere traveling parallel to the axis. Condition (i) is an approximation because z_p/a is finite while (ii) is an approximation because z/a is also finite. These approximations facilitate the use of geometric parameters from Ref. 13. As in Ref. 13 the *axial rays* which contribute to the scattering along the backward axis have a vanishing impact parameter while the impact parameters are finite for *glory rays*.

When the ray traverses are either all longitudinal ($m=0$) or all shear ($m=n$), they will be referred to as "unmixed" chords. Geometric parameters are as described in Ref. 13 with the acoustic refractive index M replaced by $M_L = c_W/c_L$ and $M_S = c_W/c_S$ for the respective cases where c_L and c_S are the bulk longitudinal and shear velocities for fused silica and c_W is the sound velocity in water. These indices depend slightly on temperature (see Sec. VII); a typical temperature was 22 °C which had $M_L = 0.2511$ and $M_S = 0.3957$. The form of ray paths with $l=1$ is illustrated in Fig. 2 which is drawn for $M=0.6$. Figure 2 also serves to define several angles and geometric parameters derived in Ref. 13. To an *external observer* located near the backward axis, the scattering appears to emanate from a virtual ringlike source, the *focal circle*.[13] The circle has a radius b and is a distance α behind the dashed vertical plane, the exit plane. (The subscript n of Ref. 13 will be omitted; here α and b depend on n, m, and l.) The angle of incidence θ which satisfies the glory condition of exact backscattering will be denoted by $\theta_{n,m,l}$. For the unmixed cases, it is given by Eq. (F17) when $l=1$ and $n=3$ or 4 and by the numerical procedure described in Ref. 13 when $n>4$. The focal-circle radius is $b=\tilde{b}a$ where

$$\tilde{b} = \sin\theta_{n,m,l}, \tag{1}$$

α is given by Eq. (F10b). Several unmixed chords, for the case of fused silica in water, are shown in Fig. 3.

When the chords are mixed, the glory condition on the angle of incidence θ is again found by considering rays traveling parallel to the axis when they are incident on the sphere and exiting from it. As in the unmixed case, b describes all of the following: the radius of the virtual source (the focal circle) and the ray's distance from the axis at impact and when in the exit plane. The generalized Snell's law and the spherical geometry give the following condition[10–12] on $\tilde{b}$

$$\pi(l-\tfrac{1}{2}) = (n-m)\arccos(\tilde{b}/M_L) + m\arccos(\tilde{b}/M_S) - \arccos(\tilde{b}). \tag{2}$$

This has been solved numerically and the glory ray's angle of

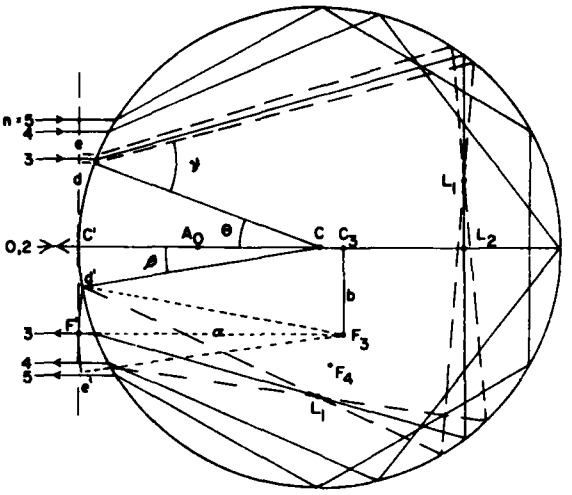

FIG. 2. Backscattered rays in a sphere representative of unmixed chord glories. When the figure is rotated about the CC' axis, the F_n trace out focal circles which are the apparent sources of backward propagating toroidal wave fronts. These waves are axially focused along the backward axis. The specular reflection appears to diverge from A_0 and is unfocused.

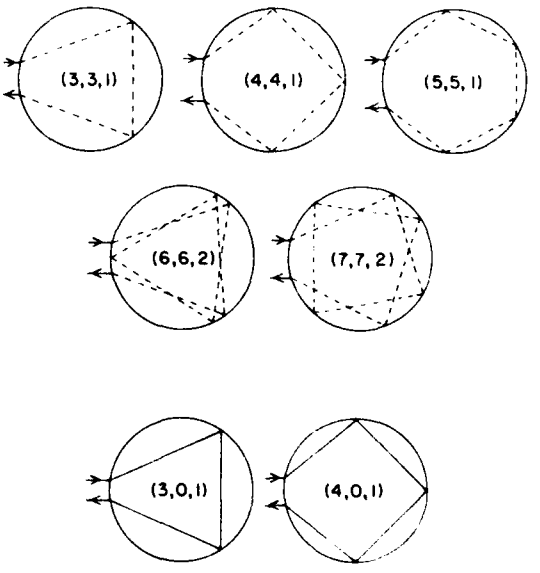

FIG. 3. Representative unmixed-chord glory rays for a fused-silica sphere in water. The parameters (n, m, l) are indicated. Dashed and solid rays represent shear and longitudinal waves, respectively.

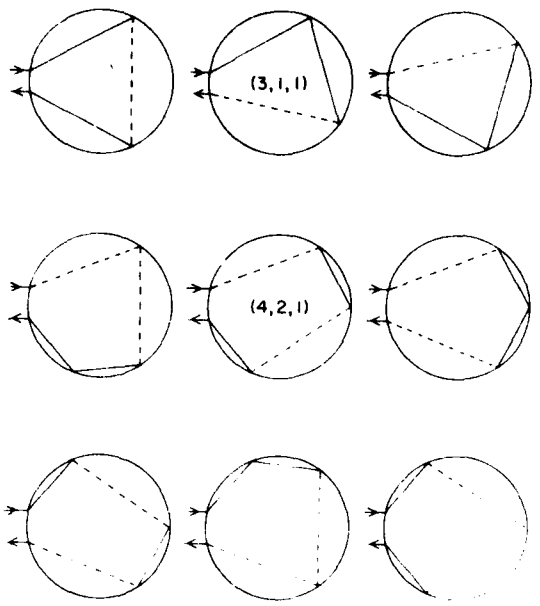

FIG. 4. Representative mixed-chord glory rays for a fused silica sphere in water. The upper and lower groups show all sequences for the (3, 1, 1) and (4, 2, 1) cases, respectively.

incidence found from (1). Snell's law gives the following condition on the internal angles ν_L and ν_S (relative to the normal at each vertex, see ν in Fig. 2) for the longitudinal and shear chords, respectively,

$$M_L \sin \nu_L = M_S \sin \nu_S = \tilde{b}. \tag{3}$$

There are $n!/[m!(n-m)!]$ different ways of ordering the chords.[11,12] Figure 4 illustrates all choices for the cases $(n, m, l) = (3, 1, 1)$ and $(4, 2, 1)$.

Consider the propagation phase shift between the crossing of the dashed vertical plane (Fig. 2) of an incoming ray and the second crossing of that plane as the ray exits. For the exactly backscattered ray, this phase shift is

$$\eta_{n,m,l} = 2ka[1 - \cos\theta_{n,m,l} + mM_S \cos\nu_S + (n-m)M_L \cos\nu_L] \tag{4}$$

in both the mixed and unmixed cases. For the mixed cases, $\eta_{n,m,l}$ (and the associated pulse delay) are independent of the ordering of the shear and longitudinal chords.[11,12] Section II demonstrates, however, the combined reflection–transmission coefficient, needed for the description of scattering amplitudes, depends on the ordering.

A dimensionless parameter q, describing the spreading of the wave front (q is the limit of the ratio of the arc lengths of $d'e'$ and de in Fig. 2 as the latter vanishes), is needed to model the scattering.[13] For unmixed chords, q is given by Eq. (F12). For the mixed chord cases, neither α nor q have been computed due to the complexities required to extend the derivation given in Appendix A of Ref. 13. Consequently, the description of mixed-chord scattering will be limited to modeling of the dependences on scattering angle and reflection–transmission factors.

II. REFLECTION AND TRANSMISSION FACTORS

To model the strength of the virtual ringlike source at each focal circle, the procedure from Ref. 13 will be followed. Reflection and transmission coefficients appropriate to an unbounded plane surface are used in conjunction with geometric factors and energy arguments. Consider an incident traveling plane wave carrying an energy E_{in} in a specified time interval. After a reflection from, or transmission through, the interface let the corresponding temporal por-

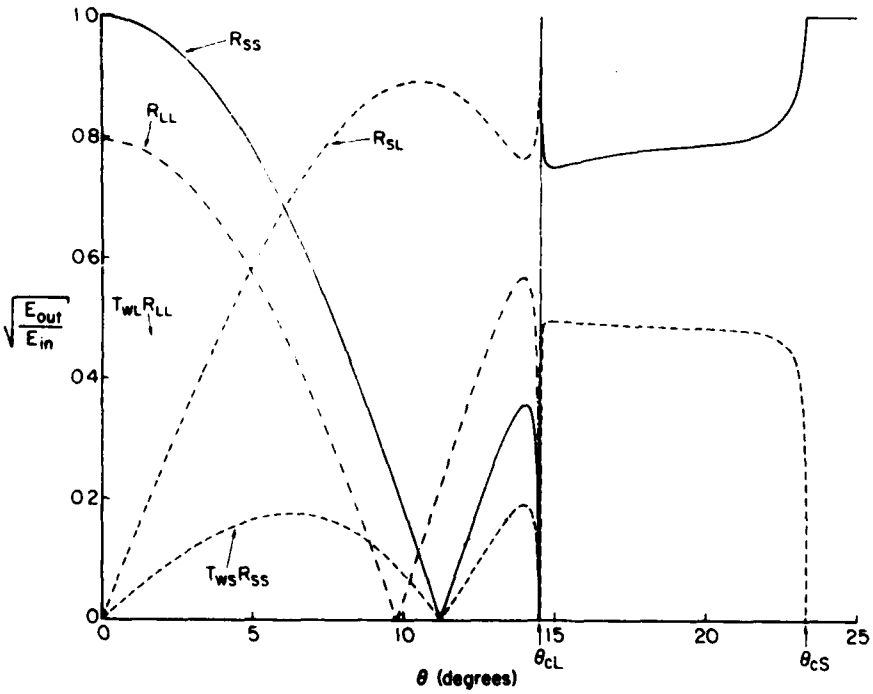

FIG. 5. Square root of the energy ratios for reflection and transmission-followed-by-reflection. These were computed for a plane water-fused silica interface. The ray in the water (which gives rise to L and S internal rays) has an angle of incidence θ.

TABLE I. Reflection and focal parameters and form functions for backscattering for selected unmixed-chord glories. The sphere is fused silica in fresh water at 22 °C.

(n, m, l)	$\theta_{n,m,l}$(deg)	R_{ij}	$T_{wj}R_{ij}$	B	α/a	q	b/a	$\lvert G_n(457, 0)\rvert$
3, 0, 1	7.77	0.27	0.14	$2.1E-2$	1.038	27.3	0.135	0.059
4, 0, 1	10.70	0.13	0.06	$4.4E-4$[a]	1.022	46.3	0.185	$1.3E-3$[a]
3, 3, 1	12.88	0.24	0.13	$1.6E-2$	1.061	17.3	0.223	0.093
4, 4, 1	17.48	0.78	0.49	$1.9E-1$	1.035	29.9	0.300	1.112
5, 5, 1	19.59	0.79	0.48	$1.5E-1$	1.022	46.5	0.335	0.779
6, 6, 2	12.11	0.13	0.06	$9.2E-6$	1.030	34.7	0.210	$3.6E-5$
7, 7, 2	14.95	0.75	0.50	$7.8E-2$	1.022	45.6	0.258	0.324

[a] $E-1$ and $E-3$ are factors of 10^{-1} and 10^{-3}, respectively, etc.

tion of the wave carry an energy E_{out}. The quantity $(E_{out}/E_{in})^{1/2}$ will be denoted by the symbols T_{ij} and R_{ij} where i and j denote the type of the incident and outgoing wave, respectively. The following subscripts are used for i and j: W for an acoustic wave in water, L for a longitudinal wave in the solid and S for a shear wave in the solid with the particle motion lying in the plane formed by the ingoing and outgoing rays. The T_{ij} and R_{ij} defined in this way are transmission and reflection coefficients which take on real values between 0 and 1; phase changes will be accounted for by a separate phase factor. The T_{ij} and R_{ij} apply to an unbounded plane wave so that complications related to the beam shifts near critical angles (e.g., the Schoch effect and Rayleigh waves) are not explicitly described in this approximation.

Expressions for the T_{ij} and R_{ij} have been derived by using boundary conditions which approximate the water as an inviscid liquid. These expressions are well known in seismology (see, e.g., Ref. 17, Eq. 7 to 17 of Ref. 18, and the review in Ref. 19). The FORTRAN computer program listed in Ref. 19 facilitates their computation with minor modifications which make it possible to set the shear wave speed of one media (the water) to zero. Results from our version of the program were checked and found to agree with standard results[18,20] over the full range of θ, the ray angle relative to the normal in the water. (Reference 20 gives R_{WW}, R_{LL}, and R_{SS} for an aluminum–water interface.) Energy conservation,[18] symmetry arguments, and numerical computations verify the following relationships

$$T_{WS} = T_{SW},\ T_{WL} = T_{LW},\ R_{LS} = R_{SL}, \tag{5}$$
$$R_{LL}^2 + R_{LS}^2 + T_{LW}^2 = 1,$$
$$R_{SS}^2 + R_{SL}^2 + T_{SW}^2 = 1,$$
$$R_{WW}^2 + T_{WS}^2 + T_{WL}^2 = 1,$$

where the ray angles θ, ν_S, and ν_L are related by the generalized Snell's law. There are critical angles of incidence θ_{cj} such that $T_{Wj} = 0$ for $\theta \geqslant \theta_{cj}$, where

$$\sin\theta_{CL} = M_L,\ \sin\theta_{cS} = M_S. \tag{6}$$

A water–fused silica interface at 22 °C has $\theta_{cL} = 14.54°$ and $\theta_{cS} = 23.31°$. For this case R_{SS}, R_{LL}, R_{SL}, and relevant products with T_{WL} and T_{WS} are shown in Fig. 5. Zeros are evident in R_{LL} near both 9.8° and θ_{cL} and in R_{SS} near both 11.2° and θ_{cL}. These features in R_{LL} and R_{SS} are discussed in detail in Ref. 18 (see, e.g., Figs. 1 and 7).

To model the virtual source strength, the product of $(E_{out}/E_{in})^{1/2}$ at each vertex is required. This may be written

$$B = T_{Wj(1)}T_{i(n+1)W}\prod_{k=2}^{n} R_{i(k)j(k)}, \tag{7}$$

where: $i(k)$ and $j(k)$ are the incident and outgoing wave types at the k th vertex; $k = 1$ corresponds to the first refraction of the incident ray; and $i(k) = j(k-1)$. We have computed B for several mixed and unmixed chords. Results for unmixed chord cases are summarized in Table I. Of these cases, the largest values of B are for those with both $m = n$ and $\theta_{n,m,l} > \theta_{cL}$.

TABLE II. Reflection and focal parameters of chord sequences for selected mixed-chord glories. The sphere is fused silica in fresh water at 22 °C.

(n, m, l)	$\theta_{n,m,l}$(deg)	b/a	B	Chord sequence
3, 1, 1	8.88	0.154	$2.1E-2$	LLS, SLL
	8.88	0.154	$1.8E-1$	LSL
3, 2, 1	10.41	0.181	$2.1E-2$	SSL, LSS
	10.41	0.181	$1.5E-1$	SLS
4, 2, 1	12.84	0.222	$1.6E-2$	LLSS, SSLL
	12.84	0.222	$9.9E-2$	LSLS, SLSL
	12.84	0.222	$1.9E-2$	LSSL
	12.84	0.222	$8.2E-2$	SLLS
5, 3, 1	14.45	0.250	$2.2E-2$	LSLSS, LSSLS, SLSSL, SSLSL
	14.45	0.250	$2.8E-3$	LLSSS, SSSLL
	14.45	0.250	$1.5E-2$	SLLSS, SSLLS
	14.45	0.250	$1.2E-1$	SLSLS
	14.45	0.250	$4.0E-3$	LSSSL

For mixed-chord glory rays having $l = 1, 2$ and $n = 3, 4$, and 5, B was computed for all $n!/[(n-m)!m!]$ chord sequences. Table II gives results for some of the rays. Evidently B depends on the sequence.[21] Sequences with mode conversion at each reflection tend to have larger B than sequences for which the L chords are grouped. For example, the largest B values of the (4, 2, 1) glory are for the LSLS and SLSL sequences; for the (5, 3, 1) glory it is the SLSLS sequence. These enhancements of B are due to the relative magnitudes of R_{SL}, R_{LL}, and R_{SS} for the relevant ray angle in the water $\theta_{n,m,l}$. The equality of the B for certain of the sequences for a given (n, m, l) can be understood via Eq. (5).

III. AMPLITUDE AND PHASE AT THE EXIT PLANE

Let $p_I \exp(-i\omega t)$ denote the incident pressure in the dashed plane through C' in Fig. 2 where ω and p_I are the frequency and amplitude of the wave. To an observer in the water, each resulting virtual source radiates a toroidal wave.[9] The amplitude in the exit plane of this outgoing wave is given by ray optics to be[13]

$$p'(s) = \frac{p_I B}{q^{1/2}} \exp\left[i\left(\eta_{n,m,l} + \mu - \Psi(s) + \frac{k(s-b)^2}{2\alpha}\right)\right], \quad (8)$$

where s is the radius in the exit plane and the parameter μ and function $\Psi(s)$ depend on n, m, l as do q, B, b, and α. The phase shift μ accounts for the phase advance of $\pi/2$ associated with each crossing of a focal curve prior to reaching the exit plane.[13] Crossings occur at points L_1 and L_2 in Fig. 2. The total μ becomes $-\pi/2$ times the number of crossings for a given (n, m, l) and ray sequence. The modulus factor B and the spreading factor q are each evaluated for rays with $\theta = \theta_{n,m,l}$; Eq. (8) neglects their dependence on s in anticipation of our use of the stationary phase approximation.

Phase changes due to transmission and reflection at each vertex are combined to give Ψ. When $\theta_{n,m,l} < \theta_{cL}$, Ψ is 0 or π and is independent of s. For unmixed shear glories having $\theta_{n,m,l} > \theta_{cL}$, the phase shift at each vertex differs from 0 or π; it depends on θ in the corresponding plane interface problem.[19] Consequently Ψ depends on s according to the original angle of incidence θ for that ray which crosses the exit plane at s. This dependence is approximated in Appendix A with the following results when $ka \gg 1$. (i) $\Psi(s)$ may be replaced by $\Psi(b)$ in Eq. (8) with b and α replaced by an *effective* focal radius b_e and distance α_e. (ii) The magnitudes of $(b - b_e)/a$ and $(\alpha - \alpha_e)/\alpha$ are roughly $(ka)^{-1}$. (iii) The corrections to b and α are so small in our experiment that they will be omitted. In the remainder of this paper (with the exception of Appendix A) Ψ will denote $\Psi(b)$.

For the mixed-chord glories, Eq. (8) describes the amplitude due to each sequence. The total amplitude for a given (n, m, l) requires that p' be summer over all chord sequences. As noted in Sec. I, the α and q have not been modeled for mixed-chord glories.

The definition of B as the product of $(E_{out}/E_{in})^{1/2}$ at each interface is such that p' is specified only for the same medium (water) in which p_I is given. Modeling of stresses within the sphere requires the use of material dependent conversion factors and it need not be described here.

IV. FARFIELD SCATTERING

In this section, the amplitude in the region $r \gg ka^2$ is considered where r is the distance from C' in Fig. 2 to the observation point (not shown) to be denoted as Q. Let the left extension of the CC' axis make an angle γ with the line $C'Q$. The Fraunhofer approximation expresses the farfield diffraction due to $p'(s)$ as a Hankel transform of $p'(s)$. The transform may be evaluated using stationary-phase and angular-spectrum techniques.[13] The farfield pressure due to a given (n, m, l) glory ray and chord sequence will be denoted by p_n. The results in Sec. IIIB of Ref. 13 become for the elastic sphere case

$$p_n(\gamma, r) = (p_I a/2r) e^{i(kr + \varphi)} G_n, \quad (9)$$

$$G_n(ka, u_n) = (ka)^{1/2} \mathscr{B} B J_0(u_n) \times \exp\left[i(\eta_{n,m,l} + \mu - \Psi - \tfrac{1}{4}\pi)\right], \quad (10)$$

$$u_n = kb \sin\gamma, \quad (11)$$

$$\varphi = -k\alpha(1 - \cos\gamma), \quad (12)$$

$$\mathscr{B} = 2b(2\pi|\alpha|/q)^{1/2} a^{-1/2}, \quad (13)$$

where for notational convenience the grouping of factors in (9) and (10) differs from that in (F28) and (F29). The significance of G_n, u_n, φ, and $\mathscr{B}$ are as follows: $G_n \exp(i\varphi)$ is the farfield form function which describes the glory amplitude relative to the geometric reflection from a fixed-rigid sphere of the same size; u_n, the argument of the zero-order Bessel function J_0 corresponds to the stationary phase point of the diffraction integral (F24) when γ is small; the phase shift φ is due to a shift of the stationary-phase point from its small-γ value; and $\mathscr{B}$ is a dimensionless geometric parameter which includes the effects of q, b, and α on the scatter amplitude. The use of the stationary-phase approximation in the diffraction integral motivated our approximation of B and q in Eq. (8) as constants evaluated at the stationary value of s which is $s = b$.

In addition to the glory contributions, axial rays also contribute to the farfield scattering. The amplitudes have the following form according to ray acoustics[13] $p_n = p_I(a/2r)\exp(ikr + i\zeta_n)f_n$, where $n = 0, 2, 4...$ is the number of internal chords and the f_n are the axial form-function moduli. The strongest amplitude is due to the first axial reflection ($n = 0$) which has $f_0 = R_{ww}$ and ζ_0 given by Eq. (F32). Here R_{ww} is the reflection coefficient evaluated with $\theta = \gamma/2$. For small values of γ, axial ravs due to shear chords are weak and only the longitudinal-chord f_n, $n = 2, 4, ...$, are significant. Geometric approximations for these f_n and an approximation for ζ_2 follow from results in Sec. IIC and Appendix C of Ref. 13.

In the geometric approximation for the axial form function moduli, the f_n are independent of ka. Consequently, if attenuation is negligible, as assumed in the derivation of (10), *glory amplitudes are enhanced by a factor proportional to* $(ka)^{1/2}$ *relative to those due to axial rays.* When $\gamma = 0°$, R_{ww} is given by the usual result for waves at normal incidence, $R_{ww} = (Z_L - Z_w)/(Z_L + Z_w)$, where the impedances $Z_L = \rho_l c_L$, $Z_w = \rho_0 c_w$, and ρ_l and ρ_0 are the densities of fused silica and water, respectively. At 22 °C, the resulting f_0 is 0.796. Comparison with the $|G_n(457,0)|$ listed in Table I

shows that the glory amplitudes exceed that due to the strongest axial ray.

V. NEARFIELD SCATTERING

In this section we extend our approximation so as to include points with $r \gg a$ which did not satisfy the previous condition $r \gg ka^2$. It is again assumed that $ka \gg 1$. The coordinate system to be used is shown in Fig. 6. The location of the origin C_n and the longitudinal coordinate z_n of the observation point Q depends on the ray parameters (n, m, l); C_n is the center of the focal circle of the (n, m, l) ray. Figure 2 shows one of these centers. With z defined as in Fig. 1, $z_n = \alpha + z$. Scalar diffraction theory[22,23] gives the following diffraction integral for the pressure p_n at Q when $r_n' \gg \lambda$

$$p_n(x,y,z_n) = \frac{1}{i\lambda}\int\int_{-\infty}^{\infty} \frac{D_n e^{ikr_n'}\delta(s-b)}{r_n'}\,dx'\,dy', \qquad (14)$$

where $s = (x'^2 + y'^2)^{1/2}$, r_n' is the distance from a point on the focal-circle's plane to Q, and D_n describes the strength of virtual source. Three approximations simplify the evaluation of (14). In the exponent take

$$r_n' \simeq z_n + [(x-x')^2 + (y-y')^2]/2z_n.$$

This is the *Fresnel approximation*[23] which is applicable provided[22]

$$z_n^3 \gg \lambda^{-1}[(x-x')^2 + (y-y')^2]^2_{\max},$$

where $x'^2 + y'^2 = b^2$. Let h denote the radial coordinate of Q' in Fig. 6. The condition becomes $z_n^3 \gg \lambda^{-1}(h+b)^4$ which for on-axis locations of the hydrophone reduces to $z_n \gg b(b/\lambda)^{1/3}$. The following approximations are less restrictive and require that $z_n \gg b$ and $z_n \gg h$. Replace r_n' in the denominator by z_n, a constant. Let the focal circle be uniform in strength[24] so that D_n does not depend on the location of Q. The integral can now be simplified by introducing the following polar coordinates: $x' = s\cos\psi$, $y' = s\sin\psi$, $x = h\cos\xi$, and $y = h\sin\xi$. Equation (14) becomes

$$p_n = \frac{D_n e^{ikz_n(1+H)}}{i\lambda z_n}\int_0^{2\pi} d\psi \int_0^{\infty} s\,ds \times \exp\left(-\frac{ik(x'x + y'y - s^2/2)}{z_n}\right)\delta(s-b), \qquad (15)$$

where $H = h^2/2z_n^2$. This expression reduces to

$$p_n(x,y,z_n) = (kbD_n/iz_n)J_0(kbh/z_n)e^{ikz_n(1+H+K)}, \qquad (16)$$

where $K = b^2/2z_n^2$ and $h/z_n = \tan\gamma_n$. For points Q not far from the axis, $z_n(1+H) \simeq r_n$, the distance from C_n to Q. To evaluate D_n we require that as $K \to 0$, $p_n(0, 0, z_n) \to p_n(\gamma = 0, r = z_n - \alpha)$ from Eq. (9). This evaluation when combined with (10) yields the following approximation for the pressure in the near- and farfields

$$p_n(x,y,z_n) = (p_I a/2z_n)\exp[ik(r_n - \alpha + z_n K)] \times G_n(ka, kbh/z_n), \qquad (17)$$

where G_n is given by (10) evaluated with $u_n = kbh/z_n$. It can be shown that when γ is not large and $r \gg kb^2$ that $k(r_n - \alpha + z_n K) \to (kr + \varphi)$. Consequently (17) reproduces the previous farfield result both on and off of the axis.

To approximate the pressure due to the axial reflection in the near field, we use the geometric result[13] that for $h/z \ll 1$, the reflection appears to come from a virtual pointlike source located a distance $a/2$ behind C'. This source is at A_0 in Fig. 2 and Ref. 13, Fig. 4. The reflected pressure at Q becomes

$$P_0 = (p_I a/2r_0)R_{ww}e^{ik(r_0 - 2^{-1}a)}, \qquad (18)$$

where r_0 is the distance from A_0 to Q and R_{ww} is evaluated at the geometric angle of incidence. From Weston's asymptotic results for electromagnetic nearfield backscattering,[25] it is expected that the leading correction to (18) will be of magnitude $(ka)^{-1}$ (or smaller) relative to unity provided r_0 is somewhat larger than $a/2$.

VI. TRANSIENT PULSES: DELAY AND DISTORTION

In this section the pressure of the incident plane wave is changed from $p_I\exp(-i\omega t)$ to a transient function of time $p_I(t)$ where the reference plane is again the dashed plane in Fig. 2. To simplify our description of the nearfield scattering, Q is now restricted to lie on the backward axis so that $x = y = 0$. After the incident wave crosses the dashed plane, the *propagation* time delay τ required to reach Q is determined by the combined k-dependent phase terms in (10) and (17):

$$\tau = \tau_0 + \tau_{n,m,l}, \qquad (19)$$

$$c_w\tau_{n,m,l} = 2a[1 - \cos\theta_{n,m,l} + mM_S\cos\nu_S + (n-m)M_L\cos\nu_L] + b^2[2(z+\alpha)]^{-1}. \qquad (20)$$

$\tau_0 = z/c_w$ is the propagation delay for the first axial reflection to reach Q. For the (n, m, l)th glory wave, $\tau_{n,m,l}$ is the delay relative to that of the axial reflection. The pressure of the first axial reflection is

$$p_0(t) = aR_{ww}(2z+a)^{-1}p_I(t - \tau_0).$$

Unlike the axial wave, the glory waves are distorted as

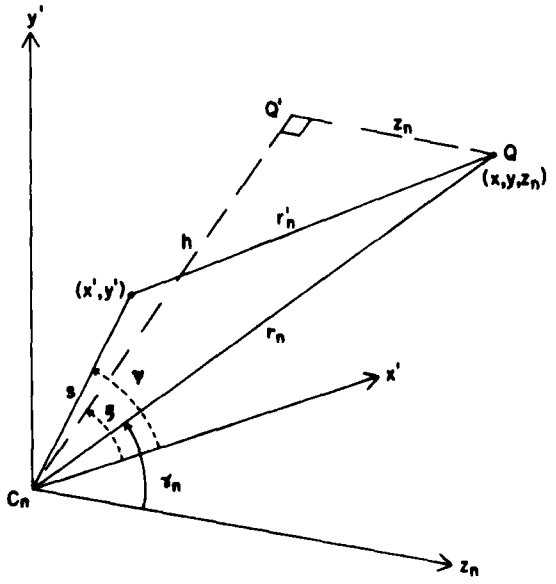

FIG. 6. Coordinate system which facilitates the description of nearfield scattering. The $x'y'$ plane contains the focal circle appropriate to the glory wave under consideration and C_n is the center of the circle.

well as shifted in time. To describe the distortion, it is convenient to define

$$\epsilon = \mu - \Psi, \tag{21}$$

where μ and Ψ are phase shifts due to internal caustics and reflection–transmission factors, respectively (Sec. III). Since $\epsilon < 0$, the phase is advanced and this k-independent shift distorts transients.[23,26,27] Further distortion is predicted as a consequence of the $k^{1/2}\exp(-i\pi/4)$ factor in (10). Appendix B models the combined distortions; combined with (17) and (19) it yields the following for the pressure of the (n, m, l)th glory wave:

$$p_n(t) = \frac{a^{3/2}\mathscr{G}B}{2z_n c_W^{1/2}}\left(\frac{d}{dt}\right)^{1/2} p_\epsilon(t-\tau), \tag{22}$$

where $(d/dt)^{1/2}$ is the *half-order derivative operator* [Eq. (B5)], p_ϵ is given by (B3) evaluated at $(t-\tau)$. In the evaluation of (B3), $p_H(t-\tau)$ is the Hilbert transform[26] of $p_I(t-\tau)$ which follows from (B4).

The phase shift by ϵ of $p_I(t-\tau)$ yields $p_\epsilon(t-\tau)$. This description of the distortion is only approximate since the shift ϵ is only applicable to spectral components having $ka \gg 1$. Application of this result to $p_I(t)$ which turn on abruptly at $t=0$ predicts precursor in p_H which extends unphysically[27] to $t = -\infty$. Due to the asymptotic limitations of (17), the resulting temporal expressions (B3) and (22) incorrectly describe the early time behavior of the precursor. In the experiment to be described the incident pressure is approximated by

$$p_I(t) = \bar{p}_I \sin(\omega t), \quad 0 < t < 2\pi N/\omega, \tag{23}$$

with $p_I(t) = 0$ elsewhere; N is an integer number of cycles, each of amplitude $\bar{p}_I$. Cron and Nuttall[26] have graphed the resulting $p_\epsilon(t)$ for $N = 1$ and 2 and various ϵ (their Figs. 2 and 4). Their analysis indicates that for integer $N \geq 2$, the *peak-to-peak* amplitude of p_ϵ in the central cycles of the tone burst is close to the undistorted value, $2\bar{p}_I$. Furthermore for these N, both the after-signal and the precursor are weak.

To estimate the effect of the half-order derivative on the peak-to-peak amplitude of the scattering we have considered $(d/dt)^{1/2} p_I$ for the p_I given by (23). When $N > 4$, the peak-to-peak amplitude of the *central cycles* of the resulting function is within 0.2% of the steady-state value $2|\omega|^{1/2}\bar{p}_I$ which follows from (B6). This steady-state approximation applies to the scattered waveform when $\sin\epsilon = 0$; however, it is to be expected that even when $\sin\epsilon \neq 0$, it approximates the peak-to-peak $(d/dt)^{1/2} p_\epsilon$ due to the aforementioned smallness of the effect of ϵ on the central peak-to-peak amplitude. The effect of the $(d/dt)^{1/2}$ operator on certain other functions has been tabulated.[28,29]

In addition to the distortions due to ϵ and the $(d/dt)^{1/2}$ operator, broadbanded signals in water are distorted due to the preferential attenuation of the high ω components. This distortion is estimated to be negligible in the experiment to be described.

VII. EXPERIMENTAL CONSIDERATIONS AND HYDROPHONE CALIBRATION

This section supplements the experiment's description given in the Introduction. We note considerations which facilitate a test of the model developed in Secs. V and VI. Figure 7 shows the scattering chamber (an $8 \times 2 \times 2\frac{1}{2}$ ft water aquarium), the transducers, and the sphere. The sphere was supported by three plastic-coated aluminum rods. (The usual practice[1,3] of hanging the target from a wire was not used due to risks of damage to the expensive sphere.) The rods were positioned so as to avoid paths of glory rays. Rod echoes were identified and eliminated using strips of anechoic rubber (not shown in Fig. 7). Echoes from the tank's rear wall were similarly eliminated. The water was filtered and deionized. The x value of the hydrophone probe (Fig. 1) was controlled by the stepper motor which is visible in Fig. 7. Rails, which extended the length of the tank, supported the driven transducer and the hydrophone positioner. The rails facilitated the location of the backward axis (the true $x = 0, y = 0$, location) to within 1 mm. Distances z_p and z were determined sonically by measuring tone-burst propagation delays with the aid of a digital delayed-pulse generator.

The hydrophone's piezoelectric element was sufficiently small (0.6 mm diam) that its directivity was insignificant for the range of x encountered in the experiment. The bent hypodermic needle which supported the hydrophone was sufficiently small in diameter (1.3 mm) that its perturbing of the incident wave was insignificant in the measurements of the glory scattering.

The source transducer (Panametrics model V309, active element diameter of $d = 12.7$ mm) was excited at frequencies below its 5-MHz resonance. It was driven by a low impedance source consisting of two matched linear 40-W power amplifiers (Amplifier Research model 40A12) operated with their outputs in parallel. The voltage $V(t)$ across the transducer was closely approximated by the function $V = \bar{V}\sin(\omega t)$ for $0 < t < 2\pi N/\omega$ and $V = 0$ all other t, where $N = 4$. This excitation was repeated at $\simeq$10-ms intervals; this interval was sufficiently long for the decay of spurious reflections. The tranducer's radiation pattern with $\omega/2\pi = 2.1$ MHz was measured near the $z = 0$ plane as a function of the impact parameter b. (This was facilitated by reversing the direction of the hydrophone from that shown in Figs. 1 and 7.) Measurements of the incident wave's amplitude $\bar{p}_I$ as a function of b (over the range of relevant b) agreed

FIG. 7. Photograph of the scattering facility. The source transducer is on the left, the bent hydrophone needle is in the center, and the sphere is on the right. Adjacent to the base of the aquarium is a rule marked in centimeters.

approximately with the elementary diffraction model of the *central* radiation pattern of a piston: $\bar{p}_l(b) \simeq \bar{p}_l(b=0)(1-b^2 v)$ where[30] $v=(kd/2z_p)^2/8$. Glory rays in our model[13] have $b \leq b_{\max} = M_S a \simeq 2.0$ cm. The resulting correction to Eq. (17) is small yet significant: $b^2_{\max} v \simeq 0.05$; it is incorporated into Eq. (24).

Figure 8 shows oscilloscope records of the first axial echo and several glory echoes. Figure 8(c) snows the axial echo, and after delays $\tau_{n,m,l} > 40\,\mu$s, several distinct glory echoes. Inspection of the time interval between the axial and glory echoes indicates that the noise amplitude is $\simeq 10\%$ of the typical echo's amplitude. Tests indicate that the principal noise source was the wideband preamplifier which was matched to the hydrophone. The preamplifier's self-noise was equivalent to an input $\simeq 2\,\mu$V rms; however, the hydrophone output voltage was small due to the combined requirements of high spatial resolution (small size of piezoelectric element) and good temporal resolution (heavily damped element for wide bandwidth). Not having signal averaging capabilities limits the extent of these experiments to measurements of echo times and (as a function of x) amplitudes but not their distortions.

Our procedure of testing Eq. (17) is to first measure the peak-to-peak preamplifier output voltage for the central cycles of the axial echo. This voltage is measured when $x = 0$; it is denoted as $\kappa P_0(x=0)$ where κ is an undetermined constant and P_0 denotes the pressure amplitude. Then, for a specific glory echo (which is identified from its $\tau_{n,m,l}$), the peak-to-peak voltage $\kappa P(x)$ is measured for the central cycles of the echo. The measurements are made from the centers of the noise broadened oscilloscope traces to facilitate a partial cancellation of noise. The result of Sec. VI is that the steady-state model is applicable to the *peak-to-peak* central portion of the glory echo's amplitude. Consequently, the model prediction for the voltage (and amplitude) ratio is

$$\frac{P(x)}{P_0(x=0)} = \frac{(z+\tfrac{1}{2}a)|G_n(ka,kbx/z_n)|(1-b^2 v)}{z_n R_{ww}}, \quad (24)$$

where the aforementioned source factor $(1-b^2 v)$ is included and R_{ww} is evaluated at normal incidence.

A technique for calibrating hydrophones which references elastic response to the amplitude of the axial reflection is described by Dragonette *et al.*[31] Our technique uses geometric and reflection factors whch differ from those of Ref. 31 in ways evident from Eqs. (18) and (24). (i) The spreading factor in the backscattered *axial* echo's amplitude is $(z+\tfrac{1}{2}a)^{-1}$, not $(z+a)^{-1}$ as it would be if the wave appeared to spread from the sphere's center. (ii) The reflected amplitude is less than that for reflection from a rigid sphere due to the coefficient R_{ww}. That the amplitude of the specular reflections is altered by a target's impedance has been confirmed previously with exact calculations of the backscattering of tone bursts, e.g., those of Davis *et al.*[32] for various rubber cylinders with $ka = 12$.

Some comments on attenuation due to bulk absorption of the 2.1 MHz bursts are in order. The bulk absorptions of shear and longitudinal waves within the fused silica are calculated to be negligible from published attenuation data even when the internal path length was long, as is the case for the (7, 7, 2) path shown in Fig. 3. [The reasons for choosing fused silica were (i) low attenuation even at high frequencies, (ii) isotropy of elastic properties, and (iii) dimensional stability.] Absorption losses within the water over the propagation distances z_p and z are not negligible if absolute amplitude is the quantity of interest. The experiments, however, yielded the *ratio* of axial and glory amplitudes. The path lengths in water of the axial and glory echoes differed by < 1 cm. Consequently these losses do not significantly alter [Eq. (24)], the model prediction.

The water temperature T varied with the room temperature. Associated with periods of rapid change in T, the glory echo amplitudes sometimes contained irregularities in their dependence on x. These irregularities were apparently due to the influence of gradients in T on the acoustic propagation. Data collection was limited to periods for which the irregularities were absent. During theses periods, measurements of $T(y)$ (via a vertical array of thermalcouples) gave vertically averaged gradients $\langle dT/dy \rangle$ having moduli < 1 °C/m though local gradients were as large as 1 °C/m.

During the series of experiments, the mean water temperature $\langle T \rangle$ ranged from 22°–25 °C. Details of the $\tau_{n,m,l}$ and $P(x)/P_0$ data were only weakly dependent on $\langle T \rangle$; however, comparisons with the theory are always made for material parameters appropriate to the T of the measurement. The

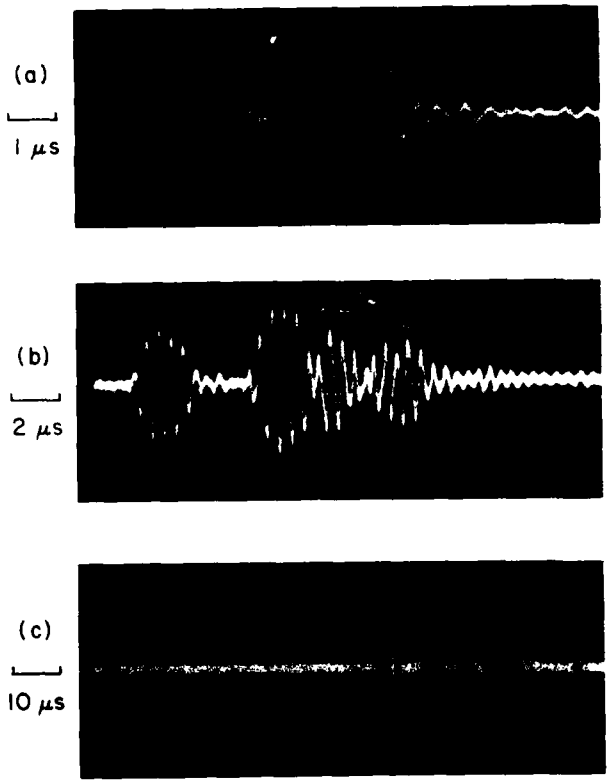

FIG. 8. Photographs of oscilloscope traces of the preamplifier output for the hydrophone on axis and $z \simeq 36$ cm. (a) Shows the first axial reflection. (b) Begins 67 μs after the axial reflection and shows several glory echoes. (c) Begins a few μs before the reflection and it shows both the reflection and the principal glory echoes. The strongest echo in (b) and (c) is the (4, 4, 1) glory echo.

fresh water data of Ref. 33 for c_W were used; e.g., at 22 °C, c_W = 1.488 km/s. Use was made of Fraser's measurements[34] of c_S and c_L for synthetic fused silicas having the normal OH ion concentration of 10^3 ppm by weight. The measurements were adjusted for T of 22° to 25 °C by using the temperature coefficients[35]: $dc_S/dT \simeq 0.28$ m/s °C and $dc_L/dT \simeq 0.68$ m/s °C. At 22 °C, this procedure gives $c_S = 3.761$ km/s and $c_L = 5.928$ km/s. The density of synthetic fused silica is 2.201 g/cm^3; at 22 °C, the density of water is 0.9978 g/cm^3.

VIII. EXPERIMENTAL RESULTS AND DISCUSSION

A. On-axis echo amplitudes and delays

We now compare measurements taken from oscilloscope traces, similar to those of Fig. 8, with the model predictions of Eqs. (20) and (24). The hydrophone was placed within 1 mm of the true backward axis. (The proximity of this axis is evident from the symmetry of off-axis amplitude data described later.) Time delays were measured from the central cycle of the axial reflection to the corresponding cycle in the glory echo. The latter time could only be determined with an uncertainty which slightly exceeded $\pm \frac{1}{2}$ cycle (± 0.24 μs). The sphere's radius was chosen to be sufficiently large that most principal glory echoes would not overlap as illustrated by Fig. 8. Representative delay and amplitude measurements for distinguishable echoes are given in Table III together with predictions. The echoes are ordered according to their delay.

The difference between the observed and modeled delay in each case was <0.5 μs. When making this comparison it should be remembered that Eq. (20) does not include the effects of the k-independent phase shift ϵ on the temporal displacement of the cycles near the center of each echo,[26] nor does it include displacements due to the $(d/dt)^{1/2}$ operator in Eq. (22). We estimate the magnitude of these apparent time shifts to be $\lesssim 0.25$ μs. The agreement of the model with these measurements facilitates the identification of these echoes.

One prominant echo appeared to be the superposition of the (5, 3, 1) and (4, 3, 1) mixed chord echoes; both are predicted to have $\tau_{n,m,l} \simeq 70.0$ μs. The resulting superposition is the first echo in Fig. 8(b). It is followed by large distinguishable echoes in Fig. 8(b) which are the (4, 4, 1) and (5, 5, 1) echoes. These are followed by a broadened echo which is a superposition of echoes for rays having $n = m > 5$ and $l = 1$.

Other than the axial reflection, Fig. 8(a), only one other axial-ray echo could be identified. This was the (2, 0, 1) echo listed in Table III which has a predicted delay $\tau_{2,0,1} = 4a/c_L$. The signal-to-noise ratio was noticeably smaller for $z = 74.4$ cm than for 36.4 cm; consequently this echo was not clearly detected in the large z case.

For the measurements with $z = 36.4$ cm, the contribution to $\tau_{n,m,l}$ of the second term on the right of Eq. (20) was as large as 0.24 μs. Evidently this term is significant since its omission decreases agreement with the data. This term has a simple physical interpretation. It approximates the time *difference* for propagation along a straight path in water from the focal circle to the hydrophone with that from the on-axis point C_n to the hydrophone. When computing this term in the mixed chord cases the exact expression for α is not known. We take $\alpha = a$ since elementary considerations indicate that the C_n lie close in the sphere's center. The values of α/a tabulated in Table I give evidence of proximity in the case of unmixed chords.

Let $\mathscr{R}_e$ and $\mathscr{R}_t$ denote the ratio of peak-to-peak amplitudes $P(x = 0)/P_0(x = 0)$ as measured and as predicted by Eq. (24), respectively. Table III compares $\mathscr{R}_e$ and $\mathscr{R}_t$ with two values of z at the indicated temperatures. For most of the echoes, $\mathscr{R}_e$ was measured on more than one day at the indicated conditions and the value is an average. With apparently similar water condition individual measurements varied by as much as ± 0.04 from the indicated $\mathscr{R}_e$. This uncertainty is also representative of comparisons among measurements taken at other temperatures. The deviations often exceeded ± 0.04 in measurements having $z = 74.4$ cm since the signal voltage was smaller relative to the amplifier's noise. Inspection of Fig. 8(a) reveals a weak signal which appears $\simeq 2$ μs after the first axial reflection. Tests indicate that this was due to the hydrophone. This signal may introduce a nonrandom source of error in the measurement of $\mathscr{R}_e$ when the echo follows an earlier echo by $\lesssim 2$ μs as is the case

TABLE III. Predicted and measured backscattering delays and amplitudes relative to those of the specular echo. The upper group was obtained with $z = 36.4$ cm and $T = 24.9$ °C. The lower group had $z = 74.4$ cm and $T = 22.0$ °C. The incident wave had $\omega/2\pi = 2.10$ MHz.

Echo	Delay $\tau_{n,m,l}$ (μs)		Ratios of peak-to-peak amplitudes		
(n, m, l)	Eq. (20)	Measured	$\mathscr{R}_t$	$\mathscr{R}_e$	$\mathscr{R}_e/\mathscr{R}_t$
2, 0, 1	34.8	34.8	0.049	0.04	0.8
3, 0, 1	44.6	44.3	0.069	0.08	1.16
3, 2, 1	62.0	62.1	...	0.54	...
4, 2, 1	63.4	63.5	...	0.70*	...
4, 4, 1	74.8	74.7	1.271	1.23	0.97
5, 5, 1	77.0	77.0	0.883	0.90	1.02
7, 7, 2	147.9	148.1	0.373	0.27	0.72
3, 0, 1	44.6	44.5	0.074	...	...
3, 1, 1	53.5	53.5	...	0.87	...
4, 4, 1	74.7	74.7	1.036	1.19	0.91
5, 5, 1	77.0	76.5	0.907	0.87	0.96
7, 7, 2	147.9	148.0	0.384	0.35	0.91

*The (4, 2, 1) amplitude may contain interference from the (5, 2, 1) echo; $\tau_{5,2,1}$ from Eq. (20) is 63.8 μs.

for (5, 5, 1).

For unmixed chord glory echoes, Eq. (24) was used to compute $\mathscr{R}_t$ and the ratios $\mathscr{R}_e/\mathscr{R}_t$ were computed. The theory overestimates the amplitudes of the glory echoes with the uncertain exceptions of (3, 0, 1) and (5, 5, 1) echoes. Note, however, that the spread of values for $\mathscr{R}_e/\mathscr{R}_t$ is *much smaller than* the spread of the $\mathscr{R}_e$. Evidently the theory correctly describes the relative ordering of glory echo amplitudes. The largest echo is the (4, 4, 1); its amplitude on the backward axis is almost as large as that for a perfectly reflecting sphere of the same size. In terms of P_0 and R_{ww} of the fused silica sphere, the perfect reflector would have $P/P_0 = (R_{ww})^{-1} \simeq 1.256$. This value is only slightly larger than the $\mathscr{R}_e$ of the (4, 4, 1) echo.

The relative values of $\theta_{n,m,l}$ and θ_{cL} significantly influence the $\mathscr{R}_t$ for those echoes with $n = m$. The (4, 4, 1), (5, 3, 1), and (7, 7, 2) glory rays all have $\theta_{n,m,l} > \theta_{cL}$. For comparison, the (3, 3, 1) echo is predicted to be small, having $\mathscr{R}_t = 0.11$. Equation (20) gives $\tau_{3,3,1} = 69.8\ \mu s$ which is close to the delays for the (5, 3, 1) and (4, 3, 1) echoes. Consequently the (3, 3, 1) echo could not be discriminated from the (5, 5, 1) and (4, 3, 1) echoes. For *aluminum* spheres in water, $\theta_{3,3,1} > \theta_{cL}$ and the (3, 3, 1) echo is predicted to be the strongest unmixed-chord glory echo.[9]

Consider now the $\mathscr{R}_e$ for the distinguishable *mixed-chord* glory echoes (3, 1, 1), (3, 2, 1), and (4, 2, 1). For each of these cases there are several chord sequences as illustrated in Fig. 4. Table II indicates that the B factor for certain of these sequences are similar in magnitude to the B of the stronger glories having $n = m$. It is consistent with our model that these three echoes were easy to detect, though their parameters α and q are not known.

Table III includes $\mathscr{R}_e$ and $\mathscr{R}_t$ for the (2, 0, 1) *axial* echo. Here $\mathscr{R}_t = (z + \frac{1}{2}a)|f_2|(z_2 R_{ww})^{-1}$ where extension of results in Appendix C of Ref. 13 to the elastic sphere case with $\theta = 0$ give the following: $|f_2| = \tilde{M} R_{ww}(1 - R_{ww}^2)$, $\tilde{M} \equiv M_L/(2 - M_L)$, $z_2 = z + \alpha_2$, and $\alpha_2/a = 1 + \frac{1}{2}\tilde{M}$. The resulting $\mathscr{R}_t$ agrees with the measured $\mathscr{R}_e$ within experimental error.

B. Off-axis echo amplitudes

The dependences of the peak-to-peak glory amplitudes on x (the displacement from the backward axis) give direct evidence of axial focusing. First consider measurements of the peak-to-peak voltage κP_0 for the simply reflected ($n = 0$) echo. The reflected wave is not axially focused. For both z of 36.4 and 74.4 cm, there was no measurable dependence of κP_0 on x for displacements $|x| \lesssim 2$ cm. In sharp contrast with this behavior, the peak-to-peak glory echo voltages κP were strongly dependent on x.

Figure 9 displays the measured ratio $P(x)/P_0(x = 0)$ associated with the (4, 4, 1) glory when $z = 36.4$ cm. The procedure which was followed was to record κP after each increment in x. Starting with $x = 0$, the scan was completed in one direction; x was reset to 0 and the scan completed in the other direction. The increments were uniform; in most scans they were 250 μm. Division of the data by $\kappa P_0(x = 0)$ yielded the plotted points. With increasing x, the echo's delay increases due to the x dependence of r_n in Eq. (17).

To find if the dependences on x is described by the steady-state model, the following quantity was graphed together with each data set:

$$\mathscr{R}_x = \mathscr{R}_e |J_0(kbx/z_n)|, \tag{25}$$

where $\mathscr{R}_e$ is the *measured* $P(0)/P_0(0)$. The x dependent factor is that of Eq. (24). Normalization to $\mathscr{R}_e$ was used since in plotted cases $\mathscr{R}_e < \mathscr{R}_t$ where $\mathscr{R}_t$ is given by (24) with $x = 0$. It is evident from Fig. 9 that (25) approximates the data except near the minima.

Most of the scans were taken with $z = 74.4$ cm where the maxima were sufficiently broad that the finite width of the hydrophone's active element (0.6 mm) was insignificant. Figures 10 and 11 give results for unmixed-chord and mixed-chord echoes, respectively. It is again evident that the echoes are localized or "focused" along the backward axis. Fluctuations of the data are larger than in Fig. 9 due to the lower amplitude of the voltages. When graphing (25) in Fig. 11, it was necessary to assume a value for α to be able to evaluate $z_n = z + \alpha$. Here we take $\alpha = a$ because of the expected proximity of the C_n to the sphere's center. The graphs in Figs. 9 and 10 use the modeled α given by Eq. (F10b). The values of $\mathscr{R}_e$ for these data sets are similar to those of Table III.

Each data set is the result of a single scan and each is plotted without smoothing. Figures 9 and 10 are representative of 11 scans of (4, 4, 1) or (5, 5, 1) echoes obtained at various water temperatures. Some comments on the symmetry of the data in Figs. 10 and 11 are merited. To symmetrize these sets, the assumed origin was shifted by 0.5 mm for all sets having $z = 74.4$ cm. This shift is consistent with the

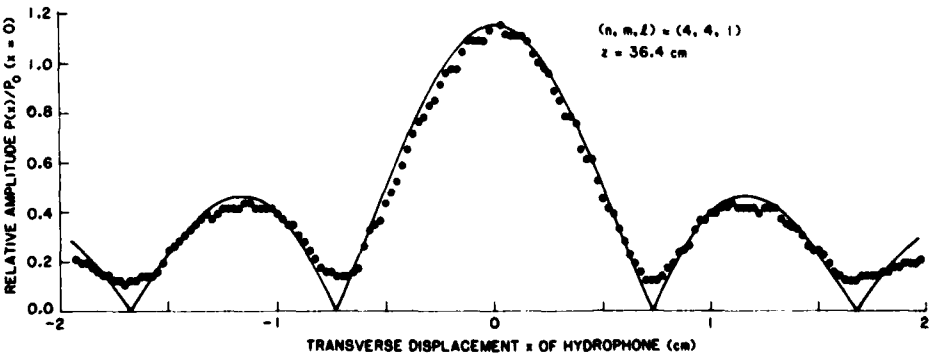

FIG. 9. The peak-to-peak voltage for the (4, 4, 1) echo plotted as a function of x. The voltages are ratioed with the on-axis value of the first axial echo. Measurements were obtained when the water temperature was 24.9 °C. The solid curve, Eq. (25), is the modeled dependence on x normalized so as to fit the measurement at $x = 0$. The peak at $x = 0$ and the side lobes are direct evidence of axial focusing.

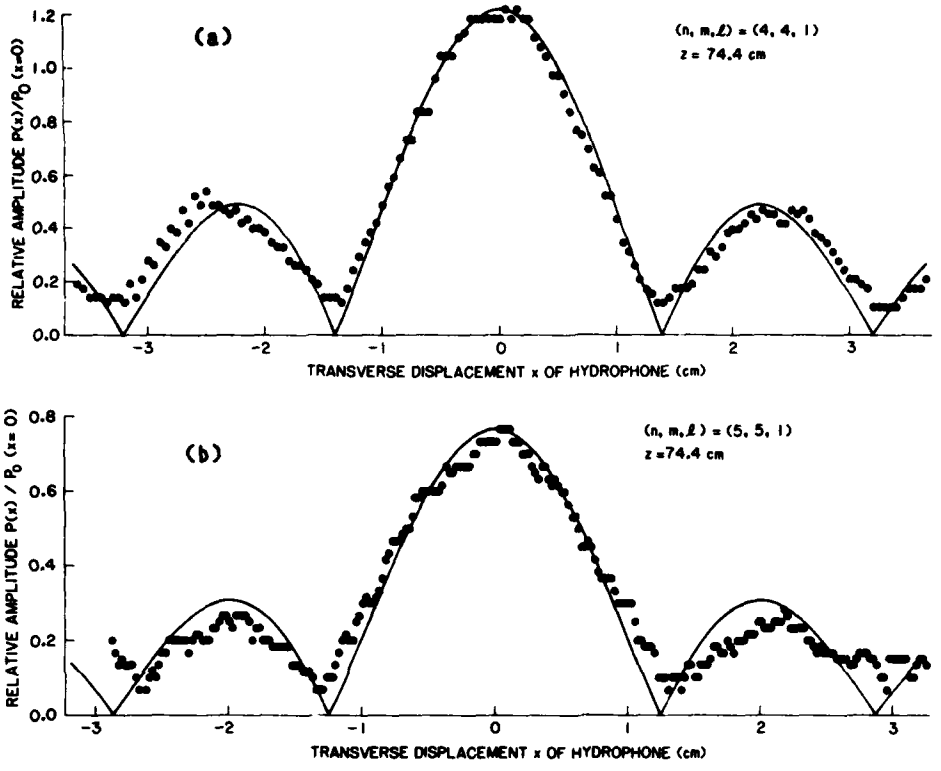

FIG. 10. Data and models (as in Fig. 9) for the (4, 4, 1) and (5, 5, 1) echoes in (a) and (b), respectively. Here $z = 74.4$ cm and the temperature was 22 °C.

aforementioned alignment imprecision. Since Figs. 10 and 11 were plotted with a common $x = 0$, $y = 0$ location, the symmetry of each data set is experimental confirmation that the different echoes are *focused along a common axis*. The predicted dependences on displacement do not depend on the azimuthal angle as a consequence of the sphere's isotropy and placement at the center of source's radiation pattern. The isotropy of the sphere was confirmed by comparing (4, 4, 1) measurements, Fig. 12, obtained before and after rotation of the sphere by an angle $\simeq 130°$.

Figures 9–11 show minima which are not as deep as predicted by the steady-state theory. Recall the assumption of $x = 0$ and $y = 0$ in the derivation of Eq. (22) and the ensuing discussion of the applicability of steady-state theory. For off-axis points, the Bessel function in Eq. (10) contains a dependence on ω not included in the derivation of (22). It is assumed in Eqs. (24) and (25) that steady-state peak-to-peak amplitudes are applicable to off-axis points *provided* the incident wave is described by Eq. (23) with $N = 4$. This assumption is suspect for x near the zeros of $J_0(kbx/z_n)$ where the dependence on ω is most significant. Careful observations of the waveform near the temporal center of the echo indicate an apparent phase shift by π as the hydrophone is scanned through each minima. This is in agreement with steady-state theory. Unfortunately, the peak-to-peak amplitudes are difficult to measure near these minima due to a small signal-to-noise ratio.

IX. CONCLUSIONS AND RELEVANCE OF PARTIAL-WAVE THEORY

We observe that the backscattering of sound from elastic spheres manifests a localized enhancement similar to that present in the optical glories of drops[14,36] and bubbles.[15] The scattering associated with particular internal rays is ob-

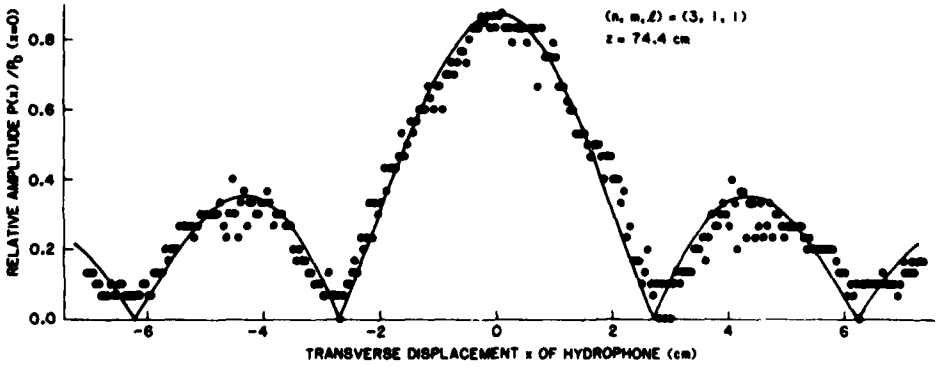

FIG. 11. Data and model (as in Fig. 9) for the (3, 1, 1) mixed-chord echo. Here $z = 74.4$ cm and the temperature was 24 °C.

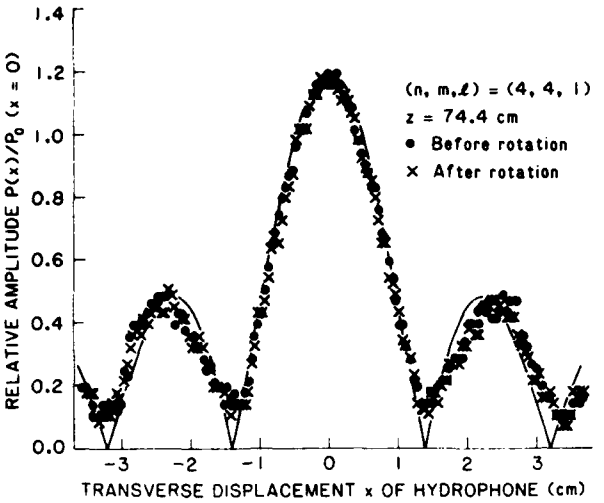

FIG. 12. Data and model (as in Fig. 9) but for $z = 74.4$ cm and a temperature of 24.7 °C. Data was obtained before and after rotation of the sphere through an angle $\simeq 130°$. The rotation axis was inclined to the backward axis; consequently the rays traversed regions of the sphere which differed before and after the rotation.

served to be axially focused. Inspection of Figs. 9–12 reveal angular widths $\Delta\gamma$ of a few degrees for the central peaks; for example in 10(a), $\Delta\gamma \simeq 2.8$ cm/$z \simeq 38$ $mr \simeq 2.2°$. The agreement with the modeled focusing pattern and the form of Eqs. (10) and (11) suggest that $\Delta\gamma \simeq u\lambda/\pi b$ radians where $u \simeq 2.4$ is the first root of $J_0(u) = 0$. This approximation should be applicable when the hydrophone's distance z and sphere's radius a are such that $z \gg a \gg \lambda$. Inspection of Figs. 10 and 11 together with Tables I and II demonstrate that the observed width of the central peak is smallest for echoes having the largest focal radii b. Inspection of Table III shows that the *discrepancy* between the observed and predicted central amplitude is approximately 5% of the predicted value. The cause of this discrepancy is not known; however, experimental difficulties due to preamplifier noise and peculiarities of the hydrophone's temporal response cannot be ruled out. The model could be refined by computing the reflection–transmission factor B along a path which accounts for the finiteness of the hydrophone and source distances, z and z_p.

Interpretation of the experiments was simplified because the short duration of the incident tone burst made possible the temporal separation of echoes with different parameters (n, m, l) in most cases. In true steady-state scattering the axial and glory echoes overlap in time. The mutual interference of these echoes would be highly dependent on ka when $ka \gg 1$. The interference of glory and axial rays due to several different parameters is the plausible cause of the ka dependent structures which are present in Flax's exact computations of backscattering from large aluminum spheres.[6] The exact farfield scattered pressure may be written in the following form[1-3] $p(\gamma, r) = (p_I a/2r)f$ where the total form function f is a sum of the partial-wave amplitudes f_j,

$$f(ka, \gamma) = \sum_{j=0}^{\infty} f_j, \tag{26}$$

$$f_j = (2/ka)U_j(ka)\mathcal{P}_j(\cos\gamma). \tag{27}$$

Here r and γ are the distance and backscattering angle relative to the sphere's center, $\mathcal{P}_j(\cos\gamma)$ is the Legendre polynomial, and U_j is a complex-valued function of ka, j, and material parameters.[1-3]

When ka is large, the axially focused backscattering amplitude due to the (n, m, l)th glory ray can be attributed to only some of the f_j. Consider the asymptotic expansion of the Legendre polynomial[37] for the case of $j \gg 1$ and $\gamma \ll 1$:

$$\mathcal{P}_j(\cos\gamma) = (\gamma/\sin\gamma)^{1/2} J_0[(j + \tfrac{1}{2})\gamma] + O(j^{-3/2}). \tag{28}$$

The dependence on γ will be similar to that of Eq. (10) provided

$$j \simeq kb - \tfrac{1}{2}. \tag{29}$$

The recognition that partial waves can be attributed to rays according to the value of the ray's impact parameter is known as the *localization principle* of optical scattering theory.[14,15,36] In the "physical-optics" approximations developed here for elastic spheres and in Ref. 13 for fluid spheres, the dominant ray-optical contributions are for those rays having impact parameters equal to the radius b of a focal circle. For values of j satisfying (29), the phases of the U_j in (27) should be stationary; consequently, there will be a significant contribution to f proportional to $J_0(kb\gamma)$. For values of j not lying close to $kb - \frac{1}{2}$ (for the b of any strong glory ray) the phases of the U_j should be such that neighboring f_j tend to cancel each other. A complete derivation of Eqs. (9) and (10) directly from the partial-wave series (26) would be complicated by the following caveats. (i) The f_j in (27) are phase referenced to the center of the sphere while Eqs. (9) and (10) are referenced to C' in Fig. 1. The two are related by the unimodular γ-dependent phase factor $\exp(i\zeta_C)$ where ζ_C is given by Eq. (F37).

(ii) Equation (9) includes an additional γ-dependent phase factor $\exp(i\varphi)$. The γ dependence of the net phase shift, $\zeta_C + \varphi = -k[2a + (\alpha - a)(1 - \cos\gamma)]$, must be preserved in any asymptotic evaluation of the partial-wave series.

Asymptotic expressions for scattering due to rays transmitted thru solid elastic cylinders were obtained by Brill and Uberall.[11] Their method used saddle-point integration to evaluate the Watson transformation of the partial wave series for *cylinders*. Unlike our results for spheres, theirs contain no $(ka)^{1/2}$ factor since backscattering from cylinders is not axially focused.

Our model predicts that backscattered transient pulses will be distorted in the manner described by Eqs. (22) and (B3)–(B6). Detection of this distortion was beyond the scope of the present experiment.

ACKNOWLEDGMENTS

Preliminary observations of the acoustic glory were described in Ref. 38. Portions of this paper were presented at the 104th meeting of the Acoustical Society of America (November 1982). This work was supported by the Office of Naval Research. One of us (P.L.M.) acknowledges the support of an Alfred P. Sloan Research Fellowship.

APPENDIX A: EFFECTS OF THE REFLECTION–TRANSMISSION PHASE SHIFTS ON FOCAL PARAMETERS

When a ray's angle of incidence in the water θ exceeds θ_{cL}, the internal rays are all shear chords. The phase changes due to transmission or reflection at each vertex vary continuously with θ. Consideration of Fig. 1 for a case in which $\theta > \theta_{cL}$ will convince the reader that outgoing wavelet $d'e'$ will be skewed so that it is no longer described by the geometric focal parameters b and a. Instead, it is described by effective parameter b_e and α_e. The purpose of this Appendix is to illustrate how $|b - b_e| \ll a$ and $|\alpha - \alpha_e| \ll \alpha$ when ka is large. The skewing is only present for glory rays having $n = m$. We simplify the notation by letting a subscript n denote the evaluation of angles or derivatives at the geometric glory condition $\theta = \theta_{n,m,l}$; henceforth, we let θ_n denote $\theta_{n,m,l}$.

Recall that s denotes the distance from C' at which a ray crosses the exit plane. Figure 2 of Ref. 13 gives an expanded view of the crossing. We are interested in rays having $\theta \simeq \theta_n$ so it is convenient to use the expansion

$$\theta - \theta_n \simeq (s-b)\left(\frac{d\theta}{ds}\right)_n + \frac{1}{2}(s-b)^2\left(\frac{d^2\theta}{ds^2}\right)_n, \tag{A1}$$

and to define the following dimensionless quantities $\theta' = a(d\theta/ds)_n$ and $\theta'' = a^2(d^2\theta/ds^2)_n$. Evaluation of Eq. (A5) of Ref. 13 at the glory condition $\theta = \beta = \theta_n$, gives $\theta' = (q\cos\theta_n)^{-1}$ where $q = \alpha/(\alpha - a)$ is the spreading factor. Inspection of Table I shows that $\theta' \ll 1$ rad. Numerical evaluation of θ'' shows that it is also small; e.g., the (4, 4, 1) ray has $\theta' \simeq 0.035$ rad and $\theta'' = -0.007$ rad.

Recall that Ψ denotes the total phase shift due to each vertex. It is convenient to use the expansion

$$\Psi - \Psi_n \simeq (\theta - \theta_n)\Psi' + \tfrac{1}{2}(\theta - \theta_n)^2\Psi'', \tag{A2}$$

where $\Psi_n = \Psi(s = b)$ in the notation of Sec. III, $\Psi' = (d\Psi/d\theta)_n$ and $\Psi'' = (d^2\Psi/d\theta^2)_n$. The constituent derivatives may be evaluated at each vertex: for example,

$$\Psi' = \left(\frac{d\Psi_{ws}}{d\theta}\right)_n + (n-1)\left(\frac{d\Psi_{ss}}{d\theta}\right)_n + \left(\frac{d\Psi_{sw}}{d\theta}\right)_n, \tag{A3}$$

where Ψ_{ss} is the shift due to reflection of a shear wave and Ψ_{ws} and Ψ_{sw} are transmission (mode-conversion) phase shifts. These shifts were computed from the complex reflection and transmission coeffcients of a plane surface[39] via the algorithm listed in Ref. 19. The Ψ' and Ψ'' were obtained numerically.

Let η denote the propagation phase delay between the entrance and exit planes, see Eq. (F7). Inspection of (8) gives $\eta - \eta_n \simeq k(s-b)^2/2\alpha$. The following *s dependence* for the total phase at the exit plane is found by combining this result with (A1) and (A2).

$$(\eta - \Psi) - (\eta_n - \Psi_n) \simeq \jmath\chi' + \tfrac{1}{2}\chi''\jmath^2, \tag{A4}$$

where $\jmath = (s-b)/a$, $\chi' = -\Psi'\theta'$, $\chi'' = ka\tilde{\alpha}^{-1} + \Lambda$, $\tilde{\alpha} = \alpha/a$, and $\Lambda = -\theta''\Psi' - \theta'^2\Psi''$. The effective focal-circle radius b_e for the *skewed wave* is the value of s for which $d(\eta - \Psi)/d\jmath = 0$; this procedure gives

$$\frac{b_e - b}{a} = \frac{-\chi'}{\chi''} = \frac{\tilde{\alpha}\Psi'\theta'}{\tilde{\alpha}\Lambda + ka}. \tag{A5}$$

The aforementioned procedure gives the following values for the (4, 4, 1) ray: $\Psi'\theta' \simeq -0.85$ and $\Lambda \simeq 0.87$ rad. Consequently, the shift of the radius is negligible when ka is large, e.g., $(b_e - b)/a \simeq -0.0019$ for $ka = 457$. These results are also representative of those for rays having θ_n closer to θ_{cs} since the θ' are smaller but the $|\Psi'|$ are larger.

The skewed wave appears to originate from a focal circle which is a distance $\alpha_e = k[d^2(\eta - \Psi)/ds^2]^{-1}$ behind the exit plane. Application of (A4) gives

$$(\alpha_e - \alpha)/\alpha = -\tilde{\alpha}\Lambda(\tilde{\alpha}\Lambda + ka)^{-1}. \tag{A6}$$

For the (4, 4, 1) ray, the shift is negligible when $ka = 457$ since $(\alpha_e - \alpha)/\alpha \simeq -0.0020$. The effective parameters influence the scattering by replacing α and b in Eqs. (10)–(13), (17), (20), (24), and in $z_n = z + \alpha$. For fused-silica spheres, the changes are negligible unless $ka \lesssim 100$.

APPENDIX B: FILTER MODEL OF PULSE DISTORTION

Inspection of the steady-state scattering amplitude, Eqs. (10) and (17) reduces the problem of the on-axis pulse distortion to answering the following question: What is the general temporal effect of a filter whose response to the function $\exp(-i\omega t)$ is $S_\omega S_\epsilon \exp(-i\omega t)$? Here S_ω and S_ϵ are the following frequency responses:

$$S_\epsilon(\omega) = \exp[i\epsilon\,\mathrm{sgn}(\omega)], \tag{B1}$$

$$S_\omega(\omega) = |\omega|^{1/2}\exp[-i\tfrac{1}{4}\pi\,\mathrm{sgn}(\omega)], \tag{B2}$$

where the function $\mathrm{sgn}(\omega) = |\omega|/\omega$ and ϵ is given by (21). In (B1) and (B2), the domain has been extended to include negative values of ω by requiring that phase advancements for positive values of ω are also advancements when ω becomes negative. The scattering process is modeled as a filter with a response S_ϵ followed by one with a response S_ω. Let $p_I(t)$ denote the input to the first filter; the output $p_\epsilon(t)$ is[26,23,40]

$$p_\epsilon(t) = p_I(t)\cos\epsilon + p_H(t)\sin\epsilon, \tag{B3}$$

where p_H is the *Hilbert transform* of p_I

$$p_H(t) = \frac{1}{\pi}P\int_{-\infty}^{\infty}\frac{p_I(t')}{(t-t')}\,dt' \tag{B4}$$

and P denotes the Cauchy principal-value integral.

It is convenient to rewrite the response of the second filter as $S_\omega = (-i\omega)^{1/2}$ where the negative real ω axis is chosen to be the branch cut in the evaluation of the radical. To obtain the temporal behavior of this filter we define the following half-order derivative operator[28]

$$\left(\frac{d}{dt}\right)^{1/2}p(t) = \int_{-\infty}^{t}\dot{p}(t')[\pi(t-t')]^{-1/2}\,dt', \tag{B5}$$

where $\dot{p}(t') = dp(t')/dt'$. By direct evaluation of (B5) it may be demonstrated that

$$\left(\frac{d}{dt}\right)^{1/2}e^{-i\omega t} = S_\omega e^{-i\omega t}. \tag{B6}$$

Application of (B6) to each of the spectral components of the input $p(t)$ to the second filter, gives the following output:

$$p_\omega(t) = \left(\frac{d}{dt}\right)^{1/2}p(t). \tag{B7}$$

Taking p to be p_ϵ lets p_ω manifest the combined effect of both

processes.

Computations of the half-order derivative of a tone burst, $(d/dt)^{1/2}p_I$ with the p_I from (23), show that the principal distortion is to the leading and trailing half-cycles.

[1]J. J. Faran, Jr., "Sound scattering by solid cylinders and spheres," J. Acoust. Soc. Am. **23**, 405–418 (1951); "Sound scattering by solid cylinders and spheres," ONR Tech. Memo. No. 22, Harvard University, Cambridge (1951).

[2]R. Hickling, "Analysis of echoes from a solid elastic sphere in water," J. Acoust. Soc. Am. **34** 1582–1592 (1962).

[3]W. G. Neubauer, R. H. Vogt, and L. R. Dragonette, "Acoustic reflection from elastic spheres. I. Steady-state signals," J. Acoust. Soc. Am. **55**, 1123–1129 (1974).

[4]L. R. Dragonette, R. H. Vogt, and W. G. Neubauer, "Acoustic reflection from elastic spheres and rigid spheres and spheroids. II. Transient analysis," J. Acoust. Soc. Am. **55**, 1130–1137 (1974).

[5]R. H. Vogt and W. G. Neubauer, "Relationship between acoustic reflection and vibrational modes of elastic spheres," J. Acoust. Soc. Am. **60**, 15–22 (1976).

[6]L. Flax, "High *ka* scattering of elastic cylinders and spheres," J. Acoust. Soc. Am. **62**, 1502–1503 (1977).

[7]L. Flax, L. R. Dragonette, and H. Uberall, "Theory of elastic resonance excitation by sound scattering," J. Acoust. Soc. Am. **63**, 723–731 (1978).

[8]S. K. Numrich, L. R. Dragonette, and L. Flax, "Classification of Submerged Targets by Acoustic Means," in *Elastic Wave Scattering and Propagation* edited by V. K. Varadan and V. V. Varadan (Ann Arbor Science, Ann Arbor, 1982), pp. 149–175.

[9]P. L. Marston and L. Flax, "Glory contributions to the backscatter from large elastic spheres," J. Acoust. Soc. Am. Suppl. 1 **68**, S81 (1980).

[10]G. J. Quentin, M. deBilly, and A. Hayman, "Comparison of backscattering of short pulses by solid spheres and cylinders at large *ka*," J. Acoust. Soc. Am. **70**, 870–878 (1981).

[11]D. Brill and H. Überall, "Acoustic waves transmitted through solid elastic cylinders," J. Acoust. Soc. Am. **50**, 921–939 (1971).

[12]P. J. Welton, M. de Billy, A. Hayman, and G. Quentin, "Backscattering of short ultrasonic pulses by solid elastic cylinders at large *ka*," J. Acoust. Soc. Am. **67**, 470–476 (1980).

[13]P. L. Marston and D. S. Langley, "Glory and rainbow enhanced acoustic backscattering from fluid spheres: Models for diffracted axial focusing," J. Acoust. Soc. Am. **73**, 1464–1475 (1983).

[14]V. Khare and H. M. Nussenzveig, "The theory of the glory," in *Statistical Mechanics and Statistical Methods in Theory and Application*, edited by U. Landman (Plenum, New York, 1977), pp. 723–764; V. Khare, "Surface waves and rainbow effects in the optical glory," in *Electromagnetic Surface Modes*, edited by A. D. Boardman (Wiley, Chichester, 1982), pp. 417–464.

[15]D. S. Langley and P. L. Marston, "Glory in optical backscattering from air bubbles," Phys. Rev. Lett. **47**, 913–916 (1981).

[16]Suprasil grade 2 manufactured by Heraeus-Amersil Inc. (Sayreville, NJ). The sphere, which has a maximum deviation from sphericity of 2.5 μm, was fabricated by Speedring Division of Schiller Industries Inc. (Cullman, AL).

[17]C. G. Knott, "Reflection and refraction of elastic waves, with seismological applications," Phil. Mag. (London) **48**, 64–97, 567–569 (1899).

[18]K. Ergin, "Energy ratio of the seismic waves reflected and refracted at a rock–water boundary," Bull. Seismol. Soc. Am. **42**, 349–372 (1952).

[19]G. B. Young and L. W. Braile, "A computer program for the application of Zoeppritz's amplitude equations and Knott's energy equations," Bull. Seismol. Soc. Am. **66**, 1881–1885 (1976).

[20]J. Krautkrämer and H. Krautkrämer, *Ultrasonic Testing of Materials* (Springer-Verlag, Berlin, 1977), pp. 605–609.

[21]This dependence on sequence is manifested more clearly in the present model than in Refs. 10–12.

[22]J. W. Goodman, *Introduction to Fourier Optics* (McGraw-Hill, San Francisco, 1968).

[23]A. D. Pierce, *Acoustics, An Introduction to its Physical Principles and Applications* (McGraw-Hill, New York, 1968).

[24]The approximation that the *virtual-source strength is independent* of Q requires that the combined reflection–transmission and spreading factors are approximately independent of θ near $\theta_{n,m,l}$. It is a questionable approximation when θ is near θ_{cL} and θ_{cS}.

[25]H. V. Weston, "Near-zone backscattering from large spheres," Appl. Sci. Res. **B9**, 107–116 (1962).

[26]B. F. Cron and A. H. Nuttal, "Phase distortion of a pulse caused by bottom reflection," J. Acoust. Soc. Am. **37**, 486–492 (1965).

[27]D. A. Sachs and S. Silbiger, "Focusing and refraction of harmonic sound and transient pulses in stratified media," J. Acoust. Soc. Am. **49**, 824–840 (1971).

[28]M. J. Lighthill, *Waves in Fluids* (Cambridge U. P., Cambridge, 1978), pp. 20–21, 86.

[29]K. B. Oldham and J. Spanier, *The Fractional Calculus* (Academic, New York, 1974), Chap. 7.

[30]A. L. Fetter and J. D. Walecka, *Theoretical Mechanics of Particles and Continua* (McGraw-Hill, New York, 1980), p. 323.

[31]L. R. Dragonette, S. K. Numrich, and L. J. Frank, "Calibration technique for acoustic scattering measurements," J. Acoust. Soc. Am. **69**, 1186–1189 (1981).

[32]C. M. Davis, L. R. Dragonette, and L. R. Flax, "Acoustic scattering from silicone rubber cylinders and spheres," J. Acoust. Soc. Am. **63**, 1694–1698 (1978).

[33]V. A. DelGrosso and C. W. Mader, "Speed of sound in pure water," J. Acoust. Soc. Am. **52**, 1442–1446 (1972).

[34]D. B. Fraser, "Factors influencing the acoustic properties of vitreous silica," J. Appl. Phys. **39**, 5868–5878 (1968).

[35]H. J. McSkimin, "Measurements of elastic constants at low temperatures by means of ultrasonic waves, data for silicon and germanium single crystals, and for fused silica," J. Appl. Phys. **24**, 988–997 (1953).

[36]H. C. Van de Hulst, "A theory of the anti-coronae," J. Opt. Soc. Am. **37**, 16–22 (1947).

[37]G. Szegö, *Orthogonal Polynomials* (American Mathematical Society, New York, 1939), Theorem 8.21.6.

[38]T. J. B. Hanson, "An acoustical backscattering experiment," M. S. Project Paper, Washington State University, 1982 (unpublished).

[39]V. Cerveny and R. Ravindra, *Theory of Seismic Head Waves* (Univ. of Toronto Press, Toronto, 1971) Sec. 2.4; W. M. Ewing, W. S. Jardetzky, and F. Press *Elastic Waves in Layered Media* (McGraw-Hill, New York, 1957), p. 79.

[40]Equation (B3) is equivalent to (7a) of Ref. 26. Our use of the $-i\omega t$ convention determines the sign on the $\sin\epsilon$ term.

Paper Number 2:
Submitted (August 1983) to J. Acoust. Soc. Am.

Half-order derivative of a sine-wave burst: Applications to two-dimensional radiation, photoacoustics, and focused scattering from spheres and a torus.

Philip L. Marston
Department of Physics
Washington State University
Pullman, WA 99164-2814

The half-order derivative $(d/dt)^{\frac{1}{2}}$ $s(t)$ is calculated for $s(t)$ given by a burst of sine waves. The burst is N cycles in length where N is an integer or a half odd-integer. The result contains Fresnel integrals; it may be written in a compact form by using the auxiliary Fresnel-integral function usually denoted by g. Some novel properties of g were derived to facilitate a discussion of the result. The calculation is applicable to several dissipationless acoustical models for which the response to an $\exp(-i\omega t)$ input is proportional to $\omega^{\frac{1}{2}}$ $\exp(-i\omega t - i\,\pi/4)$. Some examples include the pressure radiated by two-dimensional sources such as the optoacoustic radiation from a thin modulated laser beam. Another example is the pressure from virtual ring-like sources such as those present in focused backscattering from large spheres and a torus. The scattering from a large torus is modeled for the case of an incident plane wave which propagates parallel to the symmetry axis.

PACS Nos. 43.20.Px, 43.35.Sx, 43.20.Fn, 43.20.Bi

I. Introduction

This paper gives a calculation of the temporal response of certain acoustical systems to inputs consisting of bursts of sine waves. The approximate frequency responses of the systems considered, Eq. (3) below, are characterized by a 45 deg. phase advance together with a modulus which increases with the angular frequency ω in proportion to $\omega^{\frac{1}{2}}$. To describe the temporal behavior of such systems, Lighthill[1] used the following <u>half-order derivative operator</u> on the time domain function $s(t)$

$$(d/dt)^{\frac{1}{2}}\, s(t) \equiv \int_{-\infty}^{t} \dot{s}(\tau)[(t-\tau)\pi]^{-\frac{1}{2}}\, d\tau \tag{1}$$

where $\dot{s}(\tau) = ds/dt$ (evaluated at $t = \tau$). By direct evaluation of the integral, the steady-state frequency response h_ω associated with this operator is[1,2]

$$(d/dt)^{\frac{1}{2}}\, e^{-i\omega t} = h_\omega\, e^{-i\omega t}, \tag{2}$$

$$h_\omega = (-i\omega)^{\frac{1}{2}} = |\omega|^{\frac{1}{2}}\, e^{-i\frac{1}{4}\pi \mathrm{sgn}(\omega)} \tag{3}$$

where the signum function is $\mathrm{sgn}(\omega > 0) = 1$, $\mathrm{sgn}(\omega < 0) = -1$, and $\mathrm{sgn}(0) = 0$. The sine-wave bursts to be considered are N cycles in length where N is an integer or half odd-integer so the $s(t)$ are of the form

$$s_N(t) = H(\omega t)\, H(2\pi N - \omega t)\, \sin\omega t \tag{4}$$

where the Heaviside unit-step function $H(y < 0) = 0$, $H(y > 0) = 1$, and $H(y = 0) = \frac{1}{2}$. Throughout this paper we take $\omega > 0$.

Section II reviews several acoustical systems for which h_ω is an approximate transfer function for a range of ω. This response is associated with the propagation from two-dimensional sources[1] and with the effects of

diffraction in axially-focused scattering.[2] All systems considered are taken to be linear so that signal distortions due to finite amplitude effects are omitted. The effects on signal shape of the absorption of propagating sound are also omitted. The examples considered here constitute one class of intrinsic distortion. Other examples of linear problems for which distortions have been analyzed include those due to frequency independent phase shifts[3] (caused e.g. by simple caustics[4] or bottom reflections at grazing angles of incidence[5]) and those due to the focusing in stratified media.[6]

For the transients given by (4), the integral in (1) is evaluated in Sec. III. The integral also converges for other differentiable s for which $(-t)^{-\frac{1}{2}}s(t) \to 0$ as $t \to -\infty$; however, the general distorting effects of this operator will not be considered here. Though inputs proportional to (4) are not exactly realizable in physical systems, the distortions calculated should be useful in understanding properties of real systems. It is found here that the distortion is most significant near the leading and trailing edges of $(d/dt)^{\frac{1}{2}}s_N$. The operator defined in (1) is a <u>special case</u> of the "semiderivative operator" which has been used for solving the diffusion equation[7] and modeling electrochemical experiments.[8] Values of $(d/dt)^{\frac{1}{2}}s$ for some other $s(t)$ can be inferred from tables in Sec. 7.6 of Ref. 7 and in Ref. 8. Notice that <u>when</u> $s = \exp(-i\omega t)$, $(d/dt)^{\frac{1}{2}}\,(d/dt)^{\frac{1}{2}}s = ds/dt$ so the terminology <u>half-order derivative</u> is justified.

II. Some Acoustical Applications of $(d/dt)^{\frac{1}{2}}\,s(t)$

A. Pressure radiated from two-dimensional sources

Lighthill[1] considered the acoustic pressure $p(r,t)$ generated by an infinite-line thin uniform source at a perpendicular distance r from the line. The mass outflow per length of source is $s(t)$, which has units

g cm^{-1} sec^{-1}. Integrating the radiation from each line element gives the well known result

$$p(r,t) = (2\pi)^{-1} \int_r^\infty (\tilde{r}^2 - r^2)^{-\frac{1}{2}} \dot{s}(t - \tilde{r}/c) d\tilde{r} \qquad (5)$$

where c is the speed of sound in the medium. This may be simplified when s is a transient of duration Δt. In the far-zone where $r >> c\Delta t$, $(\tilde{r}^2 - r^2)$ may be replaced by $2r(\tilde{r} - r)$ so that (5) becomes[1]

$$p(r,t) \simeq (c/8\pi r)^{\frac{1}{2}} (d/dt)^{\frac{1}{2}} s(t - r/c) . \qquad (6)$$

The condition on r may be written as $r >> \tilde{\lambda}$ where $\tilde{\lambda}$ is the wavelength of the principal spectral component of $s(t)$.

Landau and Lifshitz[9] calculate the radiation from a radially vibrating infinite cylinder which has a cross-sectional area $W(t)$. The unperturbed density of the surrounding fluid is ρ_o. Their result, Eq. (73.15), is equivalent to (5) with $s(t) = \rho_o \dot{W}$ and their far-zone result, Eq. (73.17), reduces to (6). For (6) to be applicable it is necessary that $r >> \tilde{\lambda} >> W^{\frac{1}{2}}$. The continuity equation for density may be used to show that the effective mass outflow per length is indeed $\rho_o \dot{W}$.

B. Photoacoustic generation of pulsed sound in a weak optical absorber

In a review of pulsed optoacoustic spectroscopy, Patel and Tam[10] apply the Landau and Lifshitz result equivalent to (5), to the calculation of radiated pressure. The mechanism by which the pressure is generated is the heating of fluid due to the absorption of a pulsed thin light beam of radius R. The electrostrictive mechanism is neglected in their (and in the following) prediction because it is usually small.[11] Consider cylindrical coordinates for which the light beam propagates along the z axis. Let the

optical beam power at z be

$$\xi(t,z) = \xi(t,0)e^{-\alpha z} = 2\pi \int_0^R I(t,z,\tilde{r})\tilde{r}d\tilde{r}$$

where $\hat{z}I(t,z,\tilde{r})$ is the optical Poynting vector at a radius $\tilde{r}$ from the center of the assumed symmetric beam; α is the optical absorption coefficient of the fluid. In the notation of Eqs. (5) and (6), the Patel and Tam source strength prescription becomes, from Eq. (33) and (35) of Ref. 10,

$$s(t) = \alpha\beta\xi(t,0)C_p^{-1} \tag{7}$$

where β is the thermal coefficient of volume expansion and C_p is the specific heat at constant pressure. For this prescription to be applicable it is necessary that beam radius be such that[10,11]

$$R_D = (4D\Delta t)^{\frac{1}{2}} < R << c\Delta t \simeq \tilde{\lambda} \tag{8}$$

where R_D is the thermal diffusion length for the pulse duration Δt of the beam and D is the thermal diffusivity. In addition to (8), it is necessary that the pressure field at r be essentially two-dimensional so that α can't be large, $r << \alpha^{-1}$ and $z << \alpha^{-1}$; furthermore, Δt is assumed to be sufficiently long that the optical transit time across the source volume is $<< \Delta t$.

From the considerations giving (6) as the far-zone approximation to (5), it is evident that $p(r,t)$ is proportional to $(d/dt)^{\frac{1}{2}}\,\xi(t - r/c, 0)$ where the beam power ξ is evaluated at the shifted time which is r/c earlier than t. Since ξ is intrinsically positive, the calculation of $(d/dt)^{\frac{1}{2}}\,s_N$ is only applicable to photoacoustics when $N = 1/2$.

Readers not interested in focused scattering may omit Sec. IIC and IID without loss of continuity.

C. Axially-focused backscattering from spheres

Asymptotic approximations to waves backscattered from large elastic[2] and fluid spheres[12] have recently been formulated. The summary given here reviews the connection with the half-order derivative previously noted.[2] This discussion also facilitates the analysis of the backscattering from a torus given in Sec. IID. Amplitudes due to glory rays are enhanced relative to those of other reflections because of a weak axial focusing. Glory rays are defined to be backscattered rays which have non-zero impact parameters; Fig. 1 illustrates several such rays. The parameter n denotes the number of internal chords. Figure 1 displays as dashed lines, rays which lie on either side of the $n = 3$ glory ray. The wavefront associated with this glory ray corresponds to the curved wavelet d'e'. This wavefront is toroidal and it appears to emanate from a focal circle formed by rotating the point F_3 about the CC' axis. The wave is characterized by the focal parameters b, the radius of the circle, and α, the distance of the circle from the dashed vertical plane.

Let $p_I \exp(-i\omega t)$ denote the incident wave's pressure in the dashed plane through C'. The scattered pressure due to each glory ray for points on the backward axis (the left extension of the CC' axis) is computed in Ref. 2 for spheres having $ka >> 1$ where a is the sphere's radius, $k = 2\pi/\lambda$, $\lambda = 2\pi c/\omega$, and c is the sound speed in the surrounding fluid medium. It is necessary that the distance z of the observation point from C' be such that $z^3 >> \lambda^{-1} b^4$. The scattered pressure of the nth glory wave is

$$p_n = (p_I a/2z_n) \exp[ik(z + \tfrac{1}{2} b^2 z_n^{-1})] G_n \tag{9}$$

$$G_n = (ka)^{\frac{1}{2}} E B \exp[i(\eta + \varepsilon - \tfrac{1}{4}\pi)] \tag{10}$$

$$E = 2b(2\pi\alpha/q)^{\frac{1}{2}} a^{-3/2} \tag{11}$$

which correspond to Eqs. (17), (10), and (13) of Ref. 2, respectively; $z_n = z + \alpha$, B is the product of plane-surface reflection and transmission factors for each vertex [Eq. (7) of Ref. 2], and the wavelet spreading factor q is the limit of the ratio of the arc lengths of $d'e'$ and de as the latter vanishes. The phase η is the propagation delay along the glory ray. The phase $\varepsilon = \mu - \Psi$ is independent of ka (assuming $ka \gg 1$); Ψ is the combined phase of the vertex reflection an transmission coefficients. (Ψ is usually 0 or π, the exception being elastic-sphere glories for the case in which all the chords are shear wave and the angle of incidence exceeds the longitudinal critical angle.[2]) The phase μ is $-\pi/2$ times the number of internal foci crossed. Three foci are crossed for the $n = 3$ ray and these are labeled L_1 and L_2 in Fig. 1.

As a consequence of the $(ka)^{\frac{1}{2}}$ factor in (10), G_n and p_n diverge as $ka \to \infty$. This divergence is due to the axial focusing. The geometrical cause of this focusing is discussed in Ref. 12-14.

The phases in (9) and η in (10) are $\propto k$; they give rise to a time delay τ for propagation. Let $p_I(t)$ be the pressure of a transient wave incident on the dashed vertical plane. When $|\varepsilon| = 0$ or π, the frequency response in (9) and (10) is like that of (3) so the transient response is[2]

$$p_n(t) = \pm \frac{a^{3/2} EB}{2z_n c^{\frac{1}{2}}} \left(\frac{d}{dt}\right)^{\frac{1}{2}} p_I(t - \tau) \qquad (12)$$

where $+(-)$ corresponds to $|\varepsilon|$ of $0(\pi)$. For intermediate values of ε there is an additional distortion and the pressure includes a term given by the Hilbert transform[2,3] of this $p_n(t)$.

The salient feature of axially-focused backscattering is the $a^{3/2}$ proportionality in (12) whereas for simple specular reflection the

pressure $\propto a$. With appropriate focal parameters, (9) - (12) are applicable to liquid-filled spherical shells as well as elastic and liquid spheres. The internal absorption is assumed to be negligible. The cause of large target strengths observed or computed for certain liquid-filled shells[15,16] is axial focusing. This is evident since reported temporal signatures[15,16] show enhancements (relative to the specular echo) at delays of glory rays. For example, Fig. 7 and 8 of Ref. 15 display measured signatures and paths for a liquid-filled shell having an acoustical refractive index $M \approx 1.81$. The dominant echo is from an $n = 2$ glory ray which has 2 internal foci. (There is one of type L_1 and one of type L_2; see e.g. Fig. 1 of Ref. 13.) Consequently $\mu = -\pi$ and (from the impedances) $\Psi = 0$ so that $\varepsilon = -\pi$. The $(d/dt)^{\frac{1}{2}} s_N$ given in Sec. III should describe the backscattering of sine-wave bursts, however the data in Ref. 15 do not faciliate comparison.

Liquid-filled shells have potential uses as sonar calibration targets and, due to their large target strengths, as passive navigational beacons. For certain M values, G_n may increase even more rapidly than $(ka)^{\frac{1}{2}}$ so (12) is not applicable. One such case is the rainbow-enhanced glory predicted[12] to occur when $M \approx 1.18$; in that case $G_3 \propto (ka)^{2/3}$. Another example is the backward focusing of the rear axial reflection which should occur when $M = 2$. In that case, elementary diffraction and lens theory predicts $G_2 \propto ka$ when $ka \gg 1$.

D. Axially-focused backscattering from a rigid torus

Backscattered pressures proportional to $(d/dt)^{\frac{1}{2}} p_I$ are not unique to spheres. They should also exist for other shapes. In this section I extend the treatment in Sec. IIC to a new case: backscattering from a large rigid immovable torus.

Figure 2 shows the problem under consideration. The surface of the torus is generated by rotating the center of a circle C_T about the point C. The radius a of the circle is assumed to be less than the distance b which separates C_T from C. In the analysis which follows it is assumed that $ka >> 1$ and that $kb >> 1$. It is assumed that the direction of propagation of the incident plane wave is $-\hat{z}$.

The reflection of the incident wave from the rigid surface gives rise to a virtual backward-facing toroidal wavefront shown as a dashed curve in Fig. 2. The focal circle for this wave (which is at F_0) lies a distance $\alpha = a/2$ behind the dashed vertical plane. This follows from geometrical considerations similar to those[2,12] which locate the virtual point-like source of the first reflection (from a sphere) at A_0 in Fig. 1. The radius of the focal circle is b and the spreading factor q is unity. The reflection-transmission factor B is unity for the rigid torus; for real materials it is the plane-surface reflection coefficient for normal incidence.

In this analysis, multiply-reflected glory rays, such as the dotted ray in Fig. 2, will be neglected. Their contribution to the total backscattering has been estimated, Eq. (4.7) of Ref. 17, and it is small for the large torus considered here and especially for $a << b$.

Let the polar coordinates (relative to C') of the observation point be r and γ. A polar angle of $\gamma = 0°$ corresponds to backscattering. Consider the far zone in which $r >> kb^2$. The diffraction integral for this single bounce glory wave is identical to one evaluated in Sec. III of Ref. 12. When the pressure incident on the dashed vertical plane is $p_I \exp(-i\omega t)$, the scattered pressure is

$$p_0 = (p_I\, b/r)(\pi ka)^{\frac{1}{2}}\, J_0(u_0) e^{i(kr + c\varphi - \frac{1}{4}\pi)} \qquad (13)$$

where the argument of the Bessel function J_0 is $u_0 = kb \sin\gamma$ and $\varphi = -ka(1-\cos\gamma)/2$. The backscattering cross section resulting from (13) is equivalent to that for a "thick-wire loop" in the corresponding electromagnetic problem.[17,18] The frequency response of (13) with $\gamma = 0$ is like that of (3).

A more general result which includes the near zone ($z^3 >> \lambda^{-1}b^4$) is similar in form to Eqs. (9) - (12). The transient response is given by (12) with the upper sign and with the aforementioned focal parameters. These give: $B = 1$, $E = 2b\pi^{\frac{1}{2}}/a$, $z_n = z + \frac{1}{2}a$, and $c\tau = z + \frac{1}{2}b^2 z_n^{-1}$. Here z is the distance of the on-axis observation point from C'.

III. Half-order Derivative of a Sine-Wave Burst

The half-order derivative of Eq. (4) may be obtained from $I_\infty(t) = (d/dt)^{\frac{1}{2}}\, s_\infty(t)$ where $s_\infty(t) = H(\omega t)\sin\omega t$ is a burst of infinite duration which commences at $t = 0$. To evaluate (1), notice that the second term of[19] $\dot{s}_\infty = H(\omega t)\ \omega\cos\omega t + \sin\omega t(d/dt)\, H(\omega t)$ vanishes since $(d/dt)H(\omega t) = \omega\delta(\omega t)$ where $\delta(\omega t)$ is a delta function; consequently

$$I_\infty(t) = \omega\pi^{-\frac{1}{2}}\int_0^t (t-\tau)^{-\frac{1}{2}}\cos\omega\tau\, d\tau \qquad (14)$$

for $t > 0$ and $I_\infty(t<0) = 0$. Changing the integration variable to $y = (2\omega/\pi)^{\frac{1}{2}}(t-\tau)^{\frac{1}{2}}$ gives

$$I_\infty(t) = (2\omega)^{\frac{1}{2}} H(\omega t)[C(u)\cos\omega t + S(u)\sin\omega t] \qquad (15)$$

$$C(u) = \int_0^u \cos(\tfrac{\pi}{2}y^2)dy,\quad S(u) = \int_0^u \sin(\tfrac{\pi}{2}y^2)dy, \qquad (16)$$

where $u = (2\omega t/\pi)^{\frac{1}{2}}$ and C and S are Fresnel integrals. Define the following <u>auxiliary Fresnel integral function</u>[20]

$$g(u) = [\tfrac{1}{2} - C(u)]\cos(\tfrac{\pi}{2} u^2) + [\tfrac{1}{2} - S(u)]\sin(\tfrac{\pi}{2} u^2) \qquad (17)$$

and Eq. (15) becomes

$$I_\infty(t) = H(\omega t)\omega^{\frac{1}{2}}[\sin(\omega t + \tfrac{1}{4}\pi) - 2^{\frac{1}{2}} g(u)] \, . \qquad (18)$$

It is well known that as $u \to \infty$, $C(u) \to \frac{1}{2}$, $S(u) \to \frac{1}{2}$ so that $g(u) \to 0$. It is evident from (18) that for large ωt, I_∞ approaches a sine wave which is phase advanced by 45 deg and altered in magnitude by $\omega^{\frac{1}{2}}$. These steady-state properties are evident directly from (3). The expressions in (18) and (15) are in agreement with tabulated semiderivatives listed in Ref. 7 and 8 respectively.

Equation (4) may be written as $s_N(t) = s_\infty(t) \mp s_\infty(t - \omega^{-1}2\pi N)$. Here and below, for the upper (lower) sign, N is integer (half odd-integer). From the linearity of the half-order derivative operator, it follows that

$$(d/dt)^{\frac{1}{2}} s_N(t) = I_\infty(t) \mp I_\infty(t - \omega^{-1}2\pi N). \qquad (19)$$

IV. Discussion

For discussing the implications of (19), it is convenient to introduce the notations $I_N(t) = (d/dt)^{\frac{1}{2}} s_N(t)$ and $j_N(t) = \omega^{-\frac{1}{2}} I_N(t)$. Figures 3-5 display calculated j_N for $N = 4, 1$, and $\frac{1}{2}$, respectively. The calculations used the fast rational approximation to $g(u)$ given in Ref. 20 as Eq. (7.3.33). The errors due to this approximation are estimated to be negligible on the scale of these plots. When N is large, j_N closely resembles $\sin(\omega t + \frac{1}{4}\pi)$ except near its leading and trailing edges; this is especially evident on plots (not shown here) comparing j_N with $\sin(\omega t + \frac{1}{4}\pi)$. The leading maxima and minima of j_4 are ≈ 0.852, -1.032, 0.984, and -1.010. From the form of (19), these apply to other j_N for normalized times

$T = \omega t/2\pi < N$. From series expansions[20] of the Fresnel integrals in (15), it can be shown that as $T \to 0$, $j_N \propto T^{\frac{1}{2}}$ so that $j_N(t)$ vanishes with an infinite slope at $t = 0$. For a viscous fluid, the leading edge of the pressure must be rounded. For one-dimensional radiation into a viscous fluid, rounding of the leading edge has been modeled[21] for the case of a mass outflow $\propto s_\infty(t)$.

We now consider some implications for the acoustical systems discussed in Sec. II. For scattering responses describable by (12), the peak-to-peak values of the response will closely approximate the steady-state value after the first cycle. For example, the peak-to-peak values of j_4 for the four complete cycles are ≈ 1.885, 1.994, 1.998, and 1.999 which are to be compared to the steady-state value of 2. Figures in Ref. 3 show that the central peak-to-peak values of Hilbert transformed multicycle sine-wave bursts lie close to 2. These combined observations justify the use of measured peak-to-peak pressures to confirm quasi-steady-state amplitude predictions for the acoustic glory of elastic spheres.[2]

Figure 5 applies to the photoacoustic pressure radiated from a thin light beam for which the power $\xi(t,0) \propto s_{\frac{1}{2}}(t)$ and the other conditions noted in Sec. IIB hold. The maximum and minimum of $j_{\frac{1}{2}}(t)$ are ≈ 0.852 and -0.75, respectively.

The frequency response (3) vanishes at zero frequency so the following integral

$$A_N = \int_0^\infty j_N(t)dt \qquad (20)$$

must yield $A_N = 0$ for all ω in (4). Numerical integration of the computations for Fig. 3-5 gave only an approximate verification of this A_N due to the nature of the algorithm used for g. It was desirable to check

Eq. (19) by analytic evaluation of A_N. For integer N, the proof that $A_N = 0$ is trivial because the upper sign is used in (19). For half-integer values of N the proof requires an integration of g. For brevity, we consider only the case $N = \frac{1}{2}$ because the proof here can be easily generalized to N = 3/2, 5/2 . . .; integration of the sine terms in (18) and (19) give

$$\omega 2^{-\frac{1}{2}} A_{\frac{1}{2}} = 1 - 2\omega \int_0^\infty g(u)dt \qquad (21)$$

where $u = (2\omega t/\pi)^{\frac{1}{2}}$. The integral in (21) may be evaluated by first using properties[20] of the Fresnel integrals to put (17) in the following form

$$g(u) = \int_0^\infty e^{-\pi u y} \sin(\frac{\pi}{2} y^2)dy \cdot \qquad (22)$$

Inserting (22) into (21) and changing the order of the integrations yields $A_{\frac{1}{2}} = 0$ where use is made of tabulated integrals.[22] Equation (22) and the requirement that the integral in (21) yield $A_{\frac{1}{2}} = 0$ are properties of the auxiliary Fresnel-integral function g which appear to have not previously been noted.

The part of j_N for $T > N$ may be referred to as the "tail" or "wake" of the response. The result $A_N = 0$ requires the tail to be more prominent for N = 1/2, 3/2, 5/2 . . . than for integer N. It is well known[9] that pressure transients from two-dimensional sources vanish slowly as $t \to \infty$. Consider now the trailing edge for some related radiation problems. For finite-length cylindrical sources with mass outflows of finite duration, the radiated pressure will be of finite duration for a dissipationless fluid.[23] Radiation from a <u>piston</u> driven with a velocity $\propto s_1(t)$ has been modeled by Beaver[24] with the result that the pressure is of finite duration. The long tail on j_N should be suppressed in real axially-focused scattering because (12) is only applicable for spectral components having ka >> 1.

A summary of this research[25] was presented at the 105th meeting of the Acoustical Society of America. This research was supported by the Office of Naval Research and by an Alfred P. Sloan Fellowship held by P. Marston.

REFERENCES

1. J. Lighthill, Waves in Fluids (University Press, Cambridge, 1978), pp. 21, 86.
2. P. L. Marston, K. L. Williams, and T. J. B. Hanson, "Observation of the acoustic glory: High-frequency backscattering from an elastic sphere," J. Acoust. Soc. Am. 73, 605-618 (1983).
3. B. F. Cron and A. H. Nuttal, "Phase distortion of a pulse caused by bottom reflection," J. Acoust. Soc. Am. 37, 486-492 (1965).
4. A. D. Pierce, Acoustics, An Introduction to its Physical Principles and Applications (McGraw Hill, New York, 1981); D. P. Hill, "Phase shifts and pulse distortion in body waves due to internal caustics," Bull. Seism. Soc. Am. 64, 1733-1742 (1974).
5. A. B. Arons and D. R. Yennie, "Phase distortion of acoustic pulses obliquely reflected from a medium of higher sound velocity," J. Acoust. Soc. Am. 22, 231-237 (1950).
6. D. A. Sachs and A. Silbiger, "Focusing and refraction of harmonic sound and transient pulses in stratified media," J. Acoust. Soc. Am. 49, 824-840 (1971).
7. K. B. Oldham and J. Spanier, The Fractional Calculus (Academic, New York, 1974), Chap. 7.
8. K. B. Oldham and J. Spanier, "The replacement of Fick's law by a formation involving semidifferentiation," J. Electroanaly. Chem. 26, 331-341 (1970).
9. L. D. Landau and E. M. Lifshitz, Fluid Mechanics (Pergamon, London, 1959) Secs. 70, 73.
10. C. K. N. Patel and A. C. Tam, "Pulsed optoacoustic spectroscopy of condensed matter," Rev. Mod. Phys. 53, 517-550 (1981).

11. H. M. Lai and K. Young, "Theory of pulsed optoacoustic technique," J. Acoust. Soc. Am. 72, 2000-2007 (1982).

12. P. L. Marston and D. S. Langley, "Glory and rainbow-enhanced acoustic backscattering from fluid spheres: Models for diffracted axial focusing," J. Acoust. Soc. Am. 73, 1464-1475 (1983).

13. H. C. van de Hulst, "A theory of the anti-coronae," J. Opt. Soc. Am. 37, 16-22 (1947).

14. M. V. Berry, "Uniform approximation: a new concept in wave theory," Sci. Prog. (Oxford) 57, 43-64 (1969).

15. B. M. Marks and E. E. Mikeska, "Reflections from focused liquid-filled spherical reflectors," J. Acoust. Soc. Am. 59, 813-817 (1976); the reader is cautioned that in Ref. 15, the term "focused reflectors" refers to focusing of the "incident sound waves on the near back surface of the sphere" but not to the axial focusing in sense of my discussion and those in Refs. 2, 12-14.

16. D. L. Folds and C. D. Loggins, "Target strength of liquid-filled reflectors," J. Acoust. Soc. Am. 73, 1147-1151 (1983).

17. J. B. Keller and D. S. Ahluwalia, "Diffraction by a curved wire," SIAM J. Appl. Math. 20, 390-405 (1971); the reader is cautioned that here (and in Ref. 18) the definitior of a and b are reversed from those in my Fig. 2.

18. J. W. Crispin and A. L. Maffett, "Radar cross-section estimation for simple shapes," Proc. IEEE. 53, 833-848 (1965); Eq. (29).

19. M. J. Lighthill, Introduction to Fourier Analysis and Generalized Functions (Univeristy Press, Cambridge, 1958), p. 31.

20. M. Abramowitz and I. A. Stegun, Handbook of Mathematical Functions (Dover, New York, 1965), pp. 300-304.

21. D. T. Blackstock, "Transient solution for sound radiated into a viscous fluid," J. Acoust. Soc. Am. 41, 1312-1319 (1967).

22. I. S. Gradshteyn and I. M. Ryzhik, Table of Integrals, Series, and Products (Academic, New York, 1980); Entry Number 3.8521.

23. W. J. Remillard, "Pressure disturbances from a finite cylindrical source," J. Acoust. Soc. Am. 59, 744-748 (1976).

24. W. L. Beaver, "Sonic nearfields of a pulsed piston radiator," J. Acoust. Soc. Am. 56, 1043-1048 (1974).

25. P. L. Marston, "Half-order derivative of a sine-wave burst: Applications to scattering, two-dimensional radiation, and photoacoustics," J. Acoust. Soc. Am. Suppl. 73 S99 (1983).

Figure Captions

Fig. 1. Backscattered rays from a sphere for which the acoustical refractive index M = 0.6. For the 3 chord glory ray, the associated back-facing wavefront d'e' is shown together with the locations (L_1 and L_2) of internal foci. This wave is axially focused along the left extension of the CC' axis.

Fig. 2. Cross-sectional view of the torus considered in Sec. IID. The figure may be rotated about the CC' axis. The reflected wave is axially focused along the left extension of the CC' axis when the incident wave propagates in the -z direction. Scattering due to the dotted ray is omitted.

Fig. 3. The solid curve is the calculated $j_N = \omega^{-\frac{1}{2}}(d/dt)^{\frac{1}{2}}s_N$ for the 4 cycle burst given by the dashed curve. The normalized time is $T = \omega t/2\pi$.

Fig. 4. Like Fig. 3 but for N = 1.

Fig. 5. Like Fig. 3 but for N = 1/2. For real photoacoustic sources, the pressure transitions at T = 0 and 0.5 will be smoother than $j_{\frac{1}{2}}$ due to the convolution over the finite optical beam area discussed in Ref. 11.

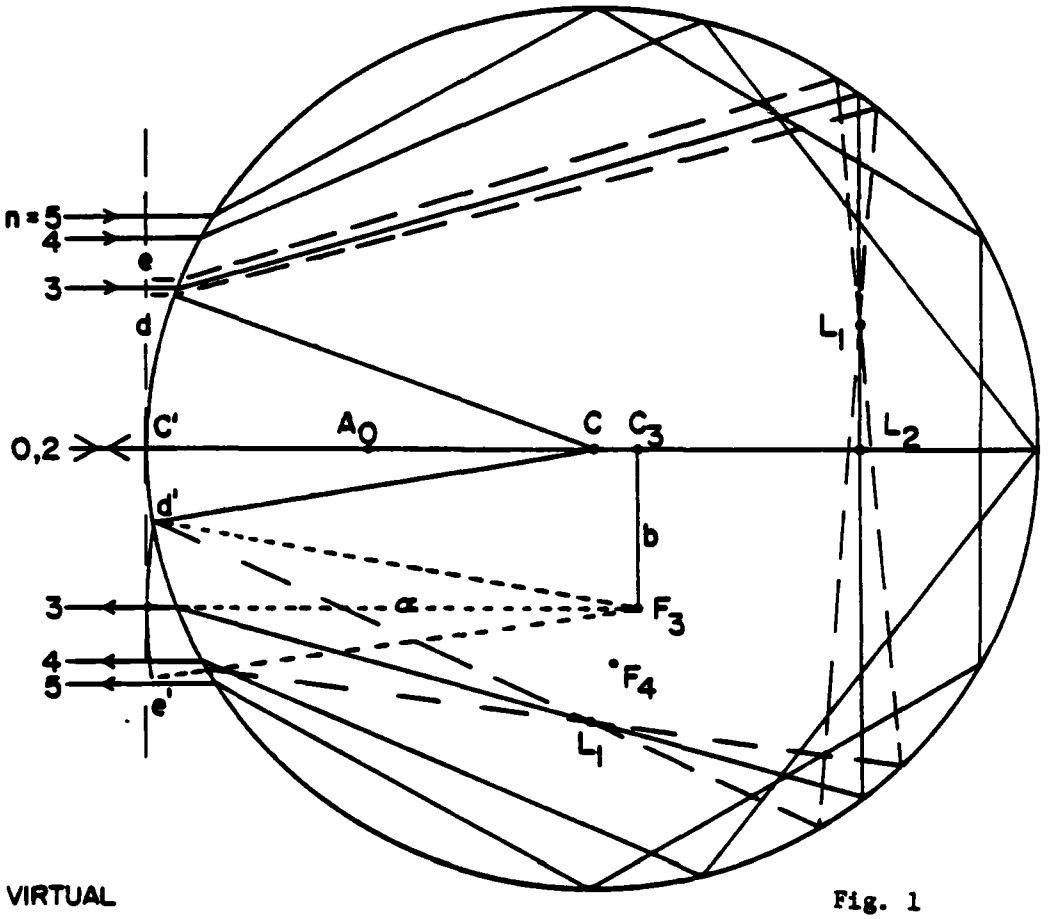
n=5
4
3
e
d
C'
A0
C
C3
L1
L2
0,2
d'
b
3
α
F3
4
5
F4
e'
L1

Fig. 1

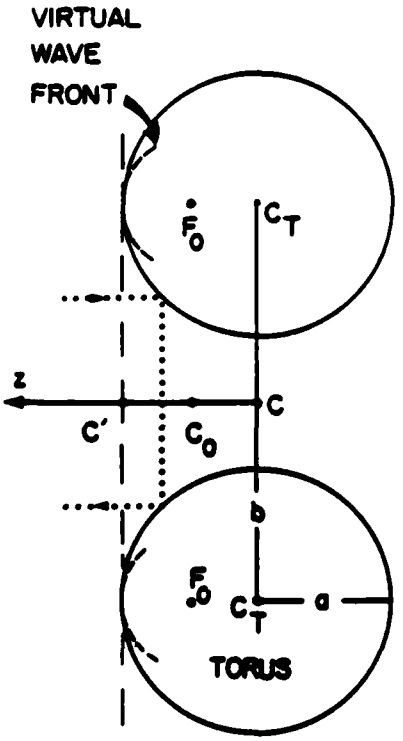
VIRTUAL
WAVE
FRONT
F0
CT
z
C
C'
C0
b
F0
CT
a
TORUS

Fig. 2

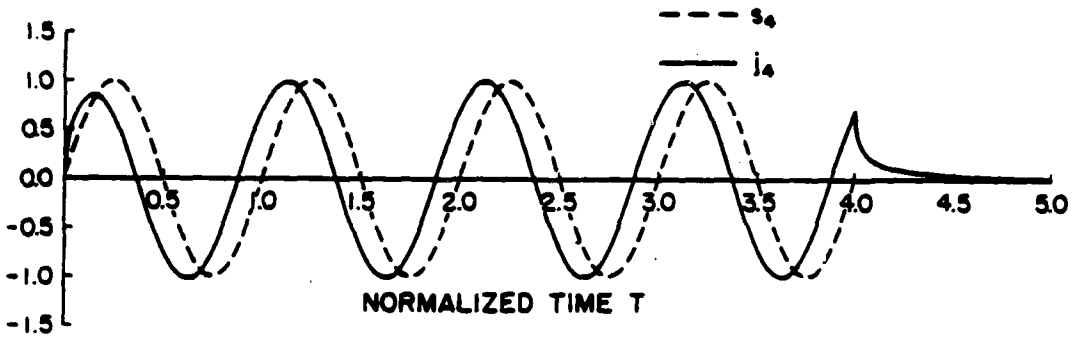

Fig. 3

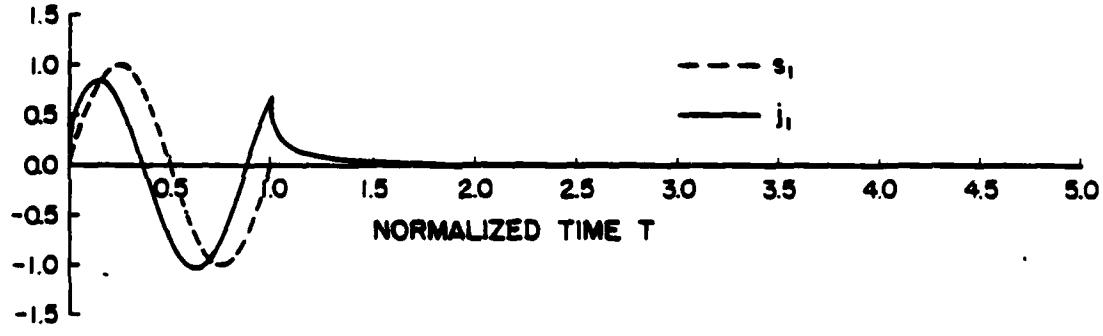

Fig. 4

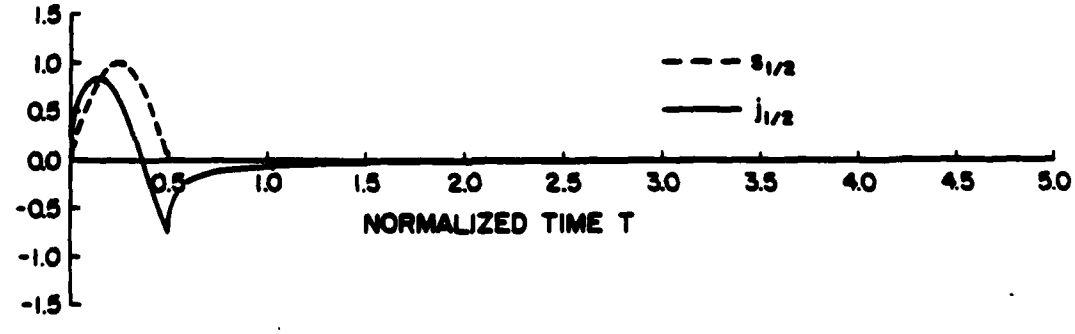

Fig. 5

Paper Number 3:

Accepted for publication in the Journal of the Optical Society of America
Submitted July, 1983

Uniform Mie-theoretic analysis of polarized and cross-polarized optical glories

Philip L. Marston
Washington State University
Department of Physics
Pullman, Washington 99164-2814

Abstract

Expressions are derived from Mie theory for the cross-polarized and non-cross-polarized measurement configurations useful for the study of the optical glories of transparent spheres.

Optical backscattering from cloud droplets,[1,2] bubbles in liquids,[3-5] and other transparent spheres[6] is enhanced due to a weak focusing along the backward axis. This enhanced scattering is referred to as the glory. Axial focusing should also enhance the forward scattering from drops[7] and from bubbles.[5] The purpose of this letter is to relate certain observable intensities with Mie theory[1,8] for the case of plane-polarized incident light. A diagram of the type of experiment under consideration is shown in Fig. 1. A sphere is illuminated with a beam propagating in the z direction having the incident E field along the x axis. The near forward or backward scattering is viewed via ideal polarizers which may be oriented to either block or pass x-polarized fields. The polarizers lie in planes which are normal to the z axis in the far-scattering zone. Previous descriptions of the transmitted intensities based on Mie theory (e.g. Eq. 6 of Ref. 4) were nonuniform in that they were applicable only near the forward or backward directions. The description presented here is not restricted by choice of angle.

It is necessary to review certain results of Mie theory. The coordinate system shown in Fig. 2(a) is equivalent to the one used in Ref. 1. At an observation point Q the orthogonal unit vectors $\underset{\sim}{e}_r$, $\underset{\sim}{e}_\theta$, and $\underset{\sim}{e}_\varphi$ are directed according to the displacement of Q with infinitesimal increases in r, θ, and φ, respectively. Let a denote the radius of the sphere and $k = 2\pi/\lambda_o$, where λ_o denotes the wavelength in the outer media (which may be a liquid in the case of scattering from bubbles). In the far zone ($r >> ka^2$), without a polarizer the scattered field is $\underset{\sim}{E}_s = E_\theta \underset{\sim}{e}_\theta + E_\varphi \underset{\sim}{e}_\varphi$ where

$$E_\theta = f S_2 \cos\varphi, \quad E_\varphi = - f S_1 \sin\varphi, \tag{1}$$

$f = (-iE_1/kr) \exp(i\omega t - ikr)$, and S_1 and S_2 are the standard Mie amplitude functions[1,9] which are to be computed for the appropriate scattering angle θ,

size parameter ka, and relative refractive index m of the sphere, and E_i is the incident wave's amplitude.

The polarizers (e.g. sheets of idealized Polaroid) do not redirect the scattered waves; consequently the local transmitted field $E_j \underset{\sim}{e}_j$ is <u>orthogonal to</u> $\underset{\sim}{e}_r$. The values for the parameter j are defined as follows. Consider the effect of polarizer 1 on a z-directed wave. If it is oriented to perfectly transmit E fields along $\underset{\sim}{e}_x$ while perfectly absorbing those along $\underset{\sim}{e}_y$, then j = 5. If it transmits E fields along $\underset{\sim}{e}_y$ while absorbing those along $\underset{\sim}{e}_x$, then j = 6. (This convention for j is justified below.) These definitions apply also to the effects of polarizer 2 on a wave directed along the -z axis. The unit vector $\underset{\sim}{e}_5$ may be constructed by removing from $\underset{\sim}{e}_x$ that part of $\underset{\sim}{e}_x$ which lies along $\underset{\sim}{e}_r$. It is

$$\underset{\sim}{e}_5 = h_5 \underset{\sim}{e}_r \times (\underset{\sim}{e}_x \times \underset{\sim}{e}_r) = h_5[\underset{\sim}{e}_x - (\underset{\sim}{e}_r \cdot \underset{\sim}{e}_x)\underset{\sim}{e}_x]$$

$$= h_5 (\underset{\sim}{e}_x - \sin\theta \cos\varphi \underset{\sim}{e}_r), \qquad (2)$$

where $h_5 = |\underset{\sim}{e}_x \times \underset{\sim}{e}_r|^{-1} = [1 - (\sin\theta \cos\varphi)^2]^{-1/2}$ and the right side of (2) follow from expressions[10] for $\underset{\sim}{e}_x$ in terms of the $\underset{\sim}{e}_r, \underset{\sim}{e}_\theta, \underset{\sim}{e}_\varphi$. Likewise, $\underset{\sim}{e}_6$ may be constructed by removing from $\underset{\sim}{e}_y$ that part of $\underset{\sim}{e}_y$ lying along $\underset{\sim}{e}_r$. It is

$$\underset{\sim}{e}_6 = h_6 \underset{\sim}{e}_r \times (\underset{\sim}{e}_y \times \underset{\sim}{e}_r) = h_6(\underset{\sim}{e}_y - \sin_\theta \sin\varphi \underset{\sim}{e}_r), \qquad (3)$$

where $h_6 = |\underset{\sim}{e}_y \times \underset{\sim}{e}_r|^{-1} = [1 - (\sin\theta \sin\varphi)^2]^{-1/2}$. In Fig. (2a), $\underset{\sim}{e}_6$ is shown. Note that for $\theta = 0$ or $\theta = \pi$ that $\underset{\sim}{e}_5 = \underset{\sim}{e}_x$ and $\underset{\sim}{e}_6 = \underset{\sim}{e}_y$.

For each case the propagating transmitted field becomes $E_j = \underset{\sim}{e}_j \cdot \underset{\sim}{E}_s$. It is convenient to define amplitude functions S_j such that

$$E_j = f S_j , \; j = 5,6, \qquad (4)$$

where the choice of values for j were selected to avoid confusion with the unrelated amplitude functions[1] S_3 and S_4 (which vanish for spheres). It is

convenient to express the S_j in terms of the standard amplitude functions S_1 and S_2 via Eqs. (1) - (3). This procedure gives

$$S_5 = h_5(S_2 \cos\theta \cos^2\varphi + S_1 \sin^2\varphi) \qquad (5)$$

$$S_6 = h_6 \sin\varphi \cos\varphi (S_2 \cos\theta - S_1). \qquad (6)$$

In agreement with elementary considerations, $\varphi = \pm\pi/2$ gives $S_5 = S_1$; also $\varphi = 0$ or π give $S_5 = S_2$ in the forward hemisphere and $S_5 = -S_2$ in the backward hemisphere.

The amplitudes S_6 and S_5 are associated with "cross-polarized" and "non-cross-polarized" scattering measurements, respectively.[3] (This definition of cross-polarization is not universally held.) When describing their associated intensities, it is convenient to use a normalization factor $I_r = I_i a^2/4r^2$ where I_i is the incident intensity and I_r is the intensity at a radius $r >> a$ for a perfectly reflecting sphere of radius a (as predicted by naive ray optics). The intensity transmitted by a j-oriented polarizer is

$$I_j = I_r \, 4|S_j|^2 (ka)^{-2}. \qquad (7)$$

For observations made in the backward hemisphere with the apparatus illustrated in Fig. 1, the (partial transmission) losses due to the beam splitter reduce the fields from those given by (1). The final result (7) is still applicable if I_r is interpreted to be the perfect reflector result with losses and the polarization dependence of the losses are negligible. A similar interpretation facilitates the application of (7) to scatterers in liquids viewed via windows with detectors (e.g. cameras) placed in air. In the latter case, the θ in (5) and (6) becomes the refracted scattering angle while the S_1 and S_2 are evaluated for a scattering angle within the liquid.

Equations (5) - (7) are the principal results of this analysis. The discussions which follow concern their application to backward and forward scattering from large transparent spheres.

To facilitate discussion of the backscattering it is convenient to use the angles illustrated in Fig. 2(b); S_1 and S_2 are evaluated at $\theta = \pi - \gamma$. Equations (5) and (6) may be written as

$$S_5 = \tfrac{1}{2}h_5[S^- - S^+ \cos 2\varphi + (1 - \cos\gamma)2S_2 \cos^2\varphi], \qquad (8)$$

$$S_6 = -\tfrac{1}{2}h_6 \sin 2\varphi\, [S^+ - (1 - \cos\gamma)S_2], \qquad (9)$$

where $S^{\pm} = S_1 \pm S_2$ appear naturally in the computation of Mie scattering,[9] $h_5 = [1 - (\sin\gamma \cos\varphi)^2]^{-1/2}$, and $h_6 = [1 - (\sin\gamma \sin\varphi)^2]^{-1/2}$. The previous approximations[4] for polarized and cross-polarized Mie scattering are given by replacing the h_j by unity and omitting the terms proportional to $(1 - \cos\gamma)$. Backward axial focusing is only significant for quite small values of γ. The angles of interest have $\gamma < 5°$ for which $(1 - \cos\gamma) < 0.004$ and the approximations introduce negligible errors. Evidently the errors should be largest for the cross-polarized case as $\gamma \to 0$, since for spheres[1] $S^+ \to 0$ though $S_2 \not\to 0$. [Representative plots of I_6 for bubbles (in which S_2 was omitted from (9)) are given in Ref. 4 and 5; the first maximum of $|S^+|$ was found to be near γ of λ_o/a rad. which is $\ll 5°$ in cases of strong backscattering. In those papers the azimuthal angle φ is denoted by ξ.] The exact and approximate I_6 vanish for $\gamma = 0$ and for $\varphi = 0, \pm\pi/2$, and π, these symmetries are evident in photographs of cross-polarized glory from bubbles;[3] I_6 manifests the glory[4] because that part of S^+ due to <u>unfocused</u> reflections is negligible when $\gamma < 5°$.

For consideration of forward scattering it is convenient to rewrite (5) and (6) as

$$S_5 = \tfrac{1}{2} h_5[S^+ - S^- \cos 2\varphi - (1 - \cos\theta) 2S_2 \cos^2\varphi], \qquad (10)$$

$$S_6 = -\tfrac{1}{2} h_6 \sin 2\varphi\,[S^- + (1 - \cos\theta) S_2], \qquad (11)$$

which show that the dependencies on S^+ and S^- are reversed from those in (8) and (9). When $\theta = 0$, I_6 vanishes since[1] $S_1 = S_2$ and $S^- = 0$. For spheres large enough for axial focusing to be significant ($ka > 200$), I_5 and I_6 are of similar magnitude in near <u>backscattering</u> but not in near <u>forward scattering</u>. The diffraction contribution to near forward scattering is (Ref. 1, p. 210)

$$(S_1)_d = (S_2)_d = \tfrac{1}{2}(S^+)_d \approx (ka)^2 \alpha^{-1} J_1(\alpha)$$

where $\alpha = ka\theta$. For comparison, the leading contribution to S^- [which from (11) is evidently the <u>intrinsic</u> cross-polarized scattering] must increase less rapidly with increasing ka; for example, transmitted toroidal wavefronts[1,3] contribute to S^- (and to S^+) in proportion to $(ka)^{3/2}$. Due to the relatively large magnitude of $(S_2)_d$, errors due to omitting the term proportional to S_2 should be more significant in (11) than in (9). Forward-directed toroidal wavefronts should manifest themselves in measured I_6; due to the non-ideal aspects of polarizers and sources, care should be taken to remove (via a spatial filter) the strong unscattered beam.

This work was supported by the Office of Naval Research and by an Alfred P. Sloan Foundation Fellowship.

REFERENCES

1. H. C. van de Hulst, Light Scattering by Small Particles (Wiley, New York, 1957).
2. V. Khare and H. M. Nussenzveig, "Theory of the glory," Phys. Rev. Lett. 38, 1279-1282 (1977).
3. D. S. Langley and P. L. Marston, "Glory in optical backscattering from air bubbles," Phys. Rev. Lett. 47, 913-916 (1981).
4. P. L. Marston and D. S. Langley, "Glory in backscattering: Mie and model predictions for bubbles and conditions on refractive index in drops," J. Opt. Soc. Am. 72, 456-459 (1982); In the final section, the equation $p\tau = -1$ should be $p\tau = 1$.
5. P. L. Marston, D. S. Langley, and D. L. Kingsbury, "Light scattering by bubbles in liquids: Mie theory, physical-optics approximations, and experiments," Appl. Sci. Res. 38, 373-383 (1982); P. L. Marston, "Light scattering by bubbles in liquids: comments and application of results to circularly polarized incident light," Appl. Sci. Res. 40, 3-5 (1983).
6. J. J. Stephens, P. S. Ray, and T. W. Kitterman, "Far-field impulse response verification of selected high-frequency optics backscattering analogs," Appl. Opt. 14, 2169-2176 (1975).
7. H. M. Nussenzveig and W. J. Wiscombe, "Forward optical glory," Opt. Lett. 5, 1279-1282 (1980).
8. G. Mie, "Beitrage zur Optik trüber Medien, speziell kolloidaler Metallösungen," Ann. Phys. (Leipzig) 25, 377-445 (1908). [English Translation No. 79-21946 (National Translation Center, Chicago, 1979)].
9. W. J. Wiscombe, "Improved Mie scattering algorithms," Appl. Opt. 19, 1505-1509 (1980).
10. G. Arfken, Mathematical Methods for Physicists, 2nd ed. (Academic, New York, 1970), p. 84.

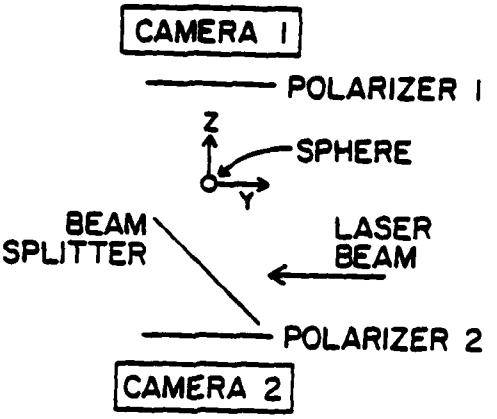

Fig. 1. Method for observing cross-polarized and non-cross-polarized scattering similar to that used in Ref. 3 for the backward glory. The diameter of the incident beam is assumed to be much larger than the sphere's diameter. The cameras are to be focused on infinity so that the photographs record the far-zone scattering. Other detectors may be used in place of cameras.

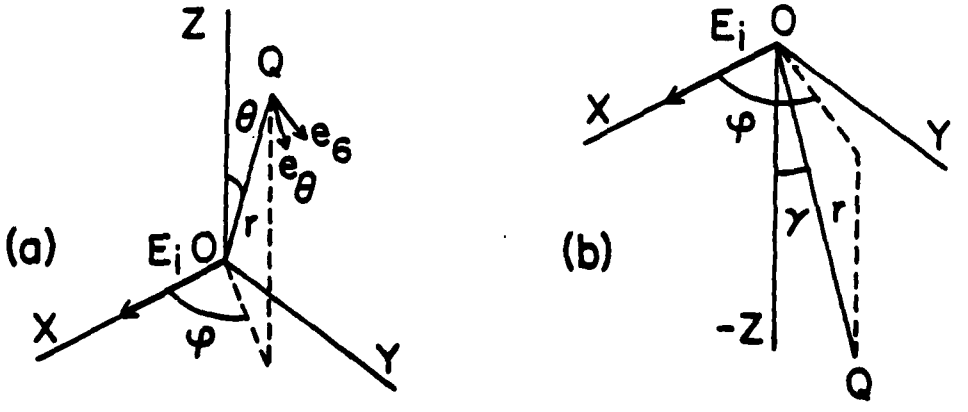

Fig. 2. Spherical coordinates used in the description of scattering to a point Q in the forward hemisphere (a) and backward hemisphere (b). The sphere is centered on O. The polarizers are in planes perpendicular to the ± z axes such that they interrupt the lines OQ when r is large.

REPORTS DISTRIBUTION LIST FOR ONR PHYSICS DIVISION OFFICE
UNCLASSIFIED CONTRACTS

Director
Defense Advanced Research Projects Agency
Attn: Technical Library
1400 Wilson Blvd.
Arlington, Virginia 22209
3 copies

Office of Naval Research
Physics Division Office (Code 412)
800 North Quincy Street
Arlington, Virginia 22217
3 copies

Office of Naval Research
Director, Technology (Code 200)
800 North Quincy Street
Arlington, Virginia 22217
1 copy

Naval Research Laboratory
Department of the Navy
Attn: Technical Library
Washington, DC 20375
1 copies

Office of the Director of Defense
Research and Engineering
Information Office Library Branch
The Pentagon
Washington, DC 20301
1 copies

U.S. Army Research Office
Box 1211
Research Triangle Park
North Carolina 27709
2 copies

Defense Technical Information Center
Cameron Station
Alexandria, Virginia 22314
12 copies

Director, National Bureau of Standards
Attn: Technical Library
Washington, DC 20234
1 copy

Commanding Officer
Office of Naval Research Western Detachment Office
1030 East Green Street
Pasadena, California 91101
1 copies

Commanding Officer
Office of Naval Research
Eastern/Central Detachment Office
495 Summer Street
Boston, Massachusetts 02210
1 copies

Commandant of the Marine Corps
Scientific Advisor (Code RD-1)
Washington, DC 20380
1 copy

Naval Ordnance Station
Technical Library
Indian Head, Maryland 20640
1 copy,

Naval Postgraduate School
Technical Library (Code 0212)
Monterey, California 93940
1 copy

Naval Missile Center
Technical Library (Code 5632.2)
Point Mugu, California 93010
1 copy

Naval Ordnance Station
Technical Library
Louisville, Kentucky 40214
1 copy

Commanding Officer
Naval Ocean Research & Development Activity
Technical Library
NSTL Station, Mississippi 39529
1 copy

Naval Explosive Ordnance Disposal Facility
Technical Library
Indian Head, Maryland 20640
1 copy

Naval Ocean Systems Center
Technical Library
San Diego, California 92152
1 copy

Naval Surface Weapons Center
Technical Library
Silver Spring, Maryland 20910
1 copy

Naval Ship Research and Development Center
Central Library (Code L42 and L43)
Bethesda, Maryland 20084
1 copy

Naval Avionics Facility
Technical Library
Indianapolis, Indiana 46218
1 copy

Director U.S. Army Engineering Research and Development Laboratories Attn: Technical Documents Center Fort Belvoir, Virginia 22060	1 copy
OUDRAE Advisory Group on Electron Devices 201 Varick Street New York, New York 10014	3 copies
Air Force Office of Scientific Research Department of the Air Force Bolling AFB, DC 22209	1 copy
Air Force Weapons Laboratory Technical Library Kirtland Air Force Base Albuquerque, New Mexico 87117	1 copy
Air Force Avionics Laboratory Air Force Systems Command Technical Library Wright-Patterson Air Force Base Dayton, Ohio 45433	1 copy
Lawrence Livermore Laboratory Attn: Dr. W. F. Krupke University of California P.O. Box 808 Livermore, California 94550	1 copy
Harry Diamond Laboratories Technical Library 2800 Powder Mill Road Adelphi, Maryland 20783	1 copy
Naval Air Development Center Attn: Technical Library Johnsville Warminster, Pennsylvania 18974	1 copy
Naval Weapons Center Technical Library (Code 753) China Lake, California 93555	1 copy
Naval Training Equipment Center Technical Library Orlando, Florida 32813	1 copy
Naval Underwater Systems Center Technical Center New London, Connecticut 06320	1 copy